On the Use of Computational Models for Wave Climate Assessment in Support of the Wave Energy Industry

by

Clayton E. Hiles
B.Eng., University of Victoria, 2007

A Dissertation Submitted in Partial Fulfillment of the Requirements for the Degree of

MASTER OF APPLIED SCIENCE

in the Department of Mechanical Engineering

On the Use of Computational Models for Wave Climate Assessment in Support of the Wave Energy Industry

by

Clayton E. Hiles
B.Eng., University of Victoria, 2007

Supervisory Committee

Dr. B. Buckham, Supervisor
(Department of Mechanical Engineering)

Dr. P. Wild, Supervisor
(Department of Mechanical Engineering)

Dr. C. Crawford, Additional Member
(Department of Mechanical Engineering)

Supervisory Committee

Dr. B. Buckham, Supervisor

(Department of Mechanical Engineering)

Dr. P. Wild, Supervisor

(Department of Mechanical Engineering)

Dr. C. Crawford, Additional Member

(Department of Mechanical Engineering)

ABSTRACT

Effective, economic extraction of ocean wave energy requires an intimate understanding of the ocean wave environment. Unfortunately, wave data is typically unavailable in the near-shore (<150m depth) areas where most wave energy conversion devices will be deployed. This thesis identifies, and where necessary develops, appropriate methods and procedures for using near-shore wave modelling software to provide critical wave climate data to the wave energy industry. The geographic focus is on the West Coast of Vancouver Island, an area internationally renowned for its wave energy development potential.

The near-shore computational wave modelling packages SWAN and REF/DIF were employed to estimate wave conditions near-shore. These models calculate wave

conditions based on the off-shore wave boundary conditions, local bathymetry and optionally, other physical input parameters. Wave boundary condition were sourced from the WaveWatchIII off-shore computational wave model operated by the National Oceanographic and Atmospheric Administration. SWAN has difficulty simulating diffraction (which can be important close to shore), but is formulated such that it is applicable over a wide range of spatial scales. REF/DIF contains a more exact handling of diffraction but is limited by computational expense to areas less than a few hundred square kilometres. For this reason SWAN and REF/DIF may be used in a complementary fashion, where SWAN is used at an intermediary between the global-scale off-shore models and the detailed, small scale computations of REF/DIF. When operating SWAN at this medium scale a number of other environmental factors become important.

Using SWAN to model most of Vancouver Island's West Coast (out to the edge of the continental shelf), the sensitivity of wave estimates to various modelling parameters was explored. Computations were made on an unstructured grid which allowed the grid resolution to vary throughout the domain. A study of grid resolution showed that a resolution close to that of the source bathymetry was the most appropriate. Further studies found that wave estimates were very sensitive to the local wind conditions and wave boundary conditions, but not very sensitive to currents or water level variations. Non-stationary computations were shown to be as accurate and more computationally efficient than stationary computations. Based on these findings it is recommended this SWAN model use an unstructured grid, operate in non-stationary mode and include wind forcing. The results from this model may be used directly to select promising wave energy development sites, or as boundary conditions to a more detailed model.

A case study of the wave climate of Hesquiaht Sound, British Columbia, Canada (a small sub-region of the medium scale SWAN model) was performed using a high resolution REF/DIF model. REF/DIF was used for this study because presence of a Hesquiaht Peninsula which has several headlands around which diffraction was thought to be important. This study estimates the most probable conditions at a number of near-shore sites on a monthly basis. It was found that throughout the year the off-shore wave power ranges from 7 to 46kW/m. The near-shore typically has 69% of the off-shore power and ranges from 5 to 39kW/m. At the near-shore site located closest to Hot Springs Cove there is on average 13.1kW/m of wave power, a significant amount likely sufficient for wave power development.

The methods implemented in this thesis may be used by groups or individuals to assess the wave climate in near-shore regions of the West Coast of Vancouver Island or other regions of the world where wave energy extraction may be promising. It is only with detailed knowledge of the wave climate that we can expect commercial extraction of wave energy to commence.

Contents

List of Tables

List of Figures

ACKNOWLEDGEMENTS

Thank you to my supervisors Dr. Buckham and Dr. Wild for their constant support, motivation and guidance. They believed in my ability as a researcher from the beginning. Thank you to Scott Beatty for bringing me on-board for the journey of wave energy research. Our cross-office discussions were not only productive but also brought humour on the days when it was needed most. Thank you to Jon Zand, Susan Boronowski, Serdar Soylu and many, many others at the UVic Department of Mechanical Engineering. The open and casual community of the Mechanical Engineering Department enriches both the academic and personal lives of its members. The biggest thank you goes to my family. They supported me in this endeavour from the start, and without them this thesis would not have been possible.

Finally, financial support has been provided by the British Columbia Innovation Council, the University of Victoria Department of Mechanical Engineering, SyncWave Energy Inc., MITACS and Triton Consultants Ltd. and is gratefully acknowledged.

For my Parents and for Dawn

Chapter 1

Introduction

The now broadly accepted realities of climate change have prompted a global search for renewable energy sources. Like wind energy, ocean wave energy is a large widely available renewable energy source that manifests through a collection of solar power. Unlike wind energy, the extraction of useful power from ocean waves has yet to prove itself commercially viable.

Extraction of wave energy is not a new idea. Patents on wave energy conversion (WEC) devices date back to the early 1800's. However, only in the last few decades has serious research utilizing modern engineering techniques allowed WEC devices to progress from conceptual ideas to operational prototypes and demonstration units. Despite this progress, the design of WEC technology has not converged in the way that wind technology has converged to a three-bladed horizontal axis design. Informed design of any WEC requires an intimate understanding of ocean waves and their characteristics. A WEC must be sited in a suitably energetic wave climate. The design and operation of a WEC must be tuned so the device can efficiently convert the most frequently encountered sea. Furthermore, an accurate resource and technology model is required to forecast the output of the device so that ancillary technologies, policy changes and strategic plans can be identified to ensure that this new energy source is effectively utilized. Wave resource assessment is an important and significant challenge facing wave energy developers.

The most promising areas for wave energy development are located near-shore, in less than 150m of water. Unfortunately, wave data is typically unavailable in this region. Even if data is available nearby a targeted development site, geographic variations in the wave climate near-shore mean it may not accurately represent the target location. Where wave data is unavailable, computational wave modelling may be used to calculate near-shore wave conditions, based on off-shore wave data. Computational wave models can also be used to overcome other challenges, such as the need for several years of data to resolve large time scale variations in the wave climate. Because WECs have a non-linear response to sea-state it is important that wave data be accurate so as not to over or under estimate WEC performance.

The geographic focus of this thesis is on the West Coast of Vancouver Island, an area internationally recognized for its potential for wave energy extraction. In order for wave energy development to move forward in this area developers will require access to high quality wave data for targeted locations. Currently no such dataset exists. To aid in correcting this deficiency this thesis provides a framework for estimating near-shore conditions, specifically on the West Coast of Vancouver Island through the use of computational wave models.

1.1 Background

This section first presents the ocean wave theory necessary to understand the character and quality of ocean wave data. It then discusses various sources of wave data, their utility and limitations. Finally the literature pertaining to wave resource assessment (WRA) in support of the wave energy industry is reviewed.

1.1.1 Ocean Surface Wave Theory

Ocean waves can be considered a stored form of solar energy. Wind is generated by differential heating of the Earth's surface by the sun. As wind blows over long stretches of open water, some of the energy in the wind is transferred to the water. The amount of energy transferred depends on the length of the stretch of water in the wind direction (*fetch*), the velocity of the wind and the duration that it blows. Waves generated in the deep oceans by off-shore storms interact little with the ocean floor and, therefore, can travel thousands of kilometres with little loss of energy. Newly generated waves tend to be high frequency, have high directional spread and are very irregular. Some of the energy in those high frequency waves is transferred to lower frequencies, or larger period, components by complex interactions between wave components called quadruplet wave-wave interactions [1]. Longer period waves travel faster than shorter period waves. Far from the source storm, hundreds of kilometres away, long period waves arrive first and the curvature of the propagating wave front is small. These two effects combine to produce long period, low directional spread waves known as *swell*. A coastal sea-state may include both high frequency wind waves and long period swell originating from multiple sources.

Ocean waves can be conveniently quantified by stochastic wave theory. A summary of the applicable theory follows; for more detail see [1, 2]. Stochastic wave theory represents a sea-state as a superposition of an infinite number of monochromatic components with distinct amplitude, frequency and direction. This yields either a one dimensional (frequency) spectrum as shown in Fig. 1.1, or a two dimensional (frequency-direction) spectrum. Both are usually expressed in terms of variance density. For convenience, a variance density spectrum may be referred to simply as a *wave spectrum*. The amount and distribution of the energy within the wave spectrum is statistically described by the parameters *significant wave height* (H_s), *peak period* (T_p) (or alternatively *energy period* (T_e)), and *peak direction* (θ_p), which are defined later in this section.

A discrete two dimensional (2D) variance density spectrum can be converted to a wave amplitude spectrum by:

$$a_{i,j} = \sqrt{2E(f_i, \theta_j)\Delta f \Delta\theta} \tag{1.1}$$

Where E is the variance density, a is the expected wave amplitude (wave height = $2a$), and Δf and $\Delta\theta$ are the bin width in frequency and direction that are centred on the values f_i and θ_i respectively. For a discrete one dimensional (1D) spectrum, the wave amplitude spectrum is given by:

$$a_i = \sqrt{2E(f_i)\Delta f} \tag{1.2}$$

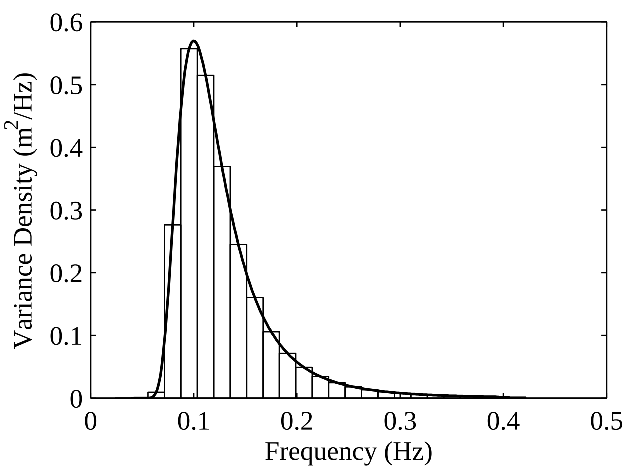

Figure 1.1: A continuous (solid line) and discrete (bars) one dimensional Pierson-Moskowitz wave spectrum for $H_s = 2$m and $T_e = 9$ sec.

The representative parameters H_s, T_p, T_e and θ_p can be calculated directly from the variance density spectrum using Eqns. (1.4-1.8). Significant wave height (H_s) is an indicator of the energy in the wave spectrum and approximates the wave height estimated by a trained observer, energy period (T_e) is the energy weighted average wave period and peak period (T_p) and peak direction (θ_p) locate the maximum value of the variance density spectrum with respect to period and direction. Perhaps the most important parameter for wave power developers is *wave power transport* (J), the power associated with one meter of wave front. For a discrete 2D variance density spectrum, wave power transport is calculated by:

$$J = \frac{1}{2}\rho g \sum_i \sum_j a_{i,j}^2 C_g(f_i, h), \tag{1.3}$$

where C_g is the *group velocity* of the wave, h is the water depth, and g is acceleration due to gravity. Group velocity, the forward velocity of a wave group, is calculated following:

$$C_g(f, h) = \frac{1}{2}\left[1 + \frac{2kh}{\sinh(2kh)}\right]\sqrt{\frac{g}{k}\tanh(kh)}. \tag{1.4}$$

The dispersion relationship must be solved iteratively to find the *wave-number*, k.

$$k = \frac{(2\pi f)^2}{g\tanh(kh)} \tag{1.5}$$

Spectral moments (m_l) are the weighted integration of the variance density spectrum where frequency to the l^{th} power is the weighting factor.

$$m_l \equiv \sum_j \sum_i f_i^l E(f_i, \theta_j)\Delta f_i \Delta\theta_j. \tag{1.6}$$

Significant wave height (H_s) is directly related to the zeroth spectral moment.

$$H_s \equiv 4\sqrt{m_0}. \tag{1.7}$$

The energy period (T_e) is defined as:

$$T_e \equiv \frac{m_{-1}}{m_0}. \tag{1.8}$$

Because H_s and T_e are calculated based on spectral moments, they vary continuously in time and are stable parameters. If two or more local maxima or 'peaks' are present in the spectrum E (see Fig. 4.6a), the evolution of the sea state may cause the global maximum of the spectrum to shift between local maxima, creating a drastic discontinuity in the variation of T_p and θ_p. For this reason they are termed unstable parameters.

1.1.2 Sources of Ocean Wave Data

Wave data is obtained by direct *in-situ* measurement, remote measurement or by calculation, based on other known environmental conditions.

Wave buoys and acoustic Doppler current profilers (ADCPs) are most commonly used to measure waves directly. Wave buoys move with the ocean surface, determining the properties of the passing waves based on those movements. Most of the larger wave buoy installations do not measure wave directionality. ADCP's are mounted to a fixed reference such as the sea floor and track the trajectory of particles in the water column. From the trajectory of those particles both currents and surface waves can be calculated. ADCP installations are often temporary as they are usually powered by batteries and do not have a means to transmit data.

Satellites can be used to measure the ocean surface remotely. Radio wave pulses are sent by the satellite, and these reflect from the sea surface. Very small *capillary* waves cause the reflected signal to scatter. Larger wind-waves cause a modulate the scattered signal and from this wave height can be calculated. Only the ocean surface directly below the satellite track can be measured and the same track is usually followed only a few times a month. As a result, measurements by satellite are poorly resolved in both space and time.

Given the appropriate wind data, wave conditions can be accurately calculated in the deep open ocean. Using finite difference methods, global wind-wave modelling software such as WaveWatchIII (WW3) and the WAve prediction Model (WAM) calculate wave generation by wind and then track the development and transformation of the resulting waves. Meteorological institutions in many nations run wave models of this type and make the data available to the public.

While direct measurements are the most accurate source of wave data, they are far from the most convenient. The purchase and maintenance costs of a single wave buoy is substantial. Furthermore, many buoys may be needed to adequately resolve the spatial variability of the wave climate in an area of interest. For Canadian and American waters there is some data available for current and past wave buoy installations, but coverage is generally not adequate for the purposes of WEC development. More useful are the results of global wind-wave models. These models are generally very accurate [3] and data is available with high spatial and temporal resolution.

1.2 Objectives of this Thesis

Near-shore computational wave models may be used to calculate near-shore wave conditions based on off-shore wave data produced by global wind-wave models. The objective of this thesis is to identify, and where necessary develop, appropriate methods and procedures for near-shore wave modelling to provide critical climate data to the wave energy industry on a site by site basis. Though generally applicable, this thesis focuses on the West Coast of Vancouver Island, an area internationally recognized for its potential for wave energy extraction. Ultimately this work will provide a framework in which a developer or contractor could quickly estimate near-shore wave conditions for a small section of coastline, using existing off-shore wave data and without running complicated global wave models. Alternatively, the tools produced could be used by a separate body to populate a database of the wave energy resource for the West Coast of Vancouver Island. Such a database does not exist and is crucial to the design of WEC's and the study of how WECs are integrated into existing electrical infrastructure and thus the search for political, social and economic support of WEC development.

This work includes:

1. *a review of suitable computational wave models and boundary condition data.*
2. *a study of the sensitivity of a medium scale near-shore model to environmental factors, solution methods and modelling options.*
3. *a case study of the near-shore wave resources near Hot Springs Cove, British Columbia, Canada*

1.3 Literature Review

The methodology for WRA has been in development since modern WEC technology research started in the early 1970's. Initial studies relied on data gathered by weather ships. Two of the first WRA executions [4, 5] used data collected by three weather ships moored around the UK to estimate the annual and seasonal energy absorption by a proposed WEC (the *Salter Duck*). A comprehensive wave climate analysis of UK waters was attempted in [6] based on measurements obtained from nine non-directional Wave Rider buoys and two observation stations. In [6] the authour acknowledged the practical need for directional and near-shore wave data and noted difficulties encountered due to temporal and spatial discontinuity of measured data. As an alternative to collection of *in-situ* measurements [7] suggests numerical wind-wave model results as a viable data source for WRA; wind-wave model results overcome all of the difficulties with measured data cited in [6] excepting near-shore data. In a study of the UK wave power resource [8] used full directional spectra from the UK MET Office numerical wind-wave model as a primary data source, and established wind-wave model results as a preferred off-shore wave data source for WRA.

The development of near-shore wave propagation software eventually allowed indirect assessment of near-shore wave energy resources based on the off-shore wave climate. For example, [9] extended on [8] to assess the near-shore wave energy resources of the UK. Five large areas of interest were identified. Average off-shore spectra were calculated at various resolutions including: each month, the summer and winter, the equinox season (April-September) and yearly. Wave ray tracing techniques were used to simulate the effect of refraction, bottom friction and breaking on a subset of individual storm spectra. Wave energy losses at selected bathymetric contours were then used to scale the average off-shore spectra, resulting in estimates of near-shore wave energy at selected sites covering the western coast of the UK.

By the early 1990's WRAs of many promising locations had been carried out but comparison of the results was difficult due to the different methods used by different authors. To address this issue, [10] developed a standard methodology for performing large-scale wave resource assessment. In [10] it is recommended that fully directional wave spectra from a numerical wind-wave model be collected for a network of off-shore reference sites with spacing at most a few hundred kilometres for a period of at least five years. To ensure accuracy, the data should then be verified against available *in-situ* measurement where possible. Upon verification, the data can be analyzed by various statistical methods to generate an atlas of off-shore wave resources. The atlas can then be used to identify regions with off-shore wave resources adequate for wave energy development. Once a target region is identified, near-shore WRA is required to further assess the merits of the location and, ultimately, to select a deployment site. Near-shore resources can be estimated through the use of numerical near-shore wave propagation software. Given the computational expense of wave propagation modelling it should only be carried out for areas of specific interest. This methodology has been utilized in full or in part by many authors since its publication [11–19]. Though developed for continental scale resource evaluation, this methodology can be effectively utilized on a small regional scale as is demonstrated in chapter 4.

Recent developments in computational models have allowed one and two-way nesting a near-shore model within an off-shore wind-wave model. In this way the fully detailed results of an off-shore computational model can be fed directly into the boundary conditions of a near-shore model. Conversely, the results calculated at the boundaries of the near-shore model may be re-applied to the global model. This nesting methodology has been applied in [20, 21]. While convenient for wave forecasts and national-scale WRA, the effort involved in developing the off-shore global scale model, the near-shore model and validating the nesting procedure may not be justified for investigation of only a small coastal region of interest to a wave energy developer.

Of specific interest to Canadian waters are [22] and [13]. Presented in [22] is a wave atlas for Canadian waters based on buoy measurements and WW3 hind-casts. [13] extends on [22] to perform a near-shore wave climate study for the Pacific Rim National Park of Vancouver Island, BC, Canada. Spectra were synthesized for 388 sea-states covering the entire range of H_s, T_p and θ_p occurrences in a WW3 hind-cast data set. Those sea-states were then propagated through the near-shore domain using near-shore wave modelling software. The near-shore results were then interpolated at each 3 hour period in the off-shore WW3 data set to create a near-shore hind-cast. On average the near-shore hind-cast corresponds reasonably well to near-shore measurements made by a directional wave buoy deployed independent of the modelling project.

1.4 Research Path and Thesis Organization

The geographic focus of this thesis is on the West Coast of Vancouver Island. The potential of this area for wave energy extraction is internationally recognized, but realization of that potential will require that those interested in deploying WEC devices have access to high quality wave climate data. Currently no such data set exists for Vancouver Island. To aid in correcting this deficiency this thesis provides a framework for estimating near-shore conditions, specifically on the West Coast of Vancouver Island though the use of computational wave models.

The basis of this framework is the off-shore wave data produced by global-scale computational models which is freely available in the public domain. Chapter 2 discusses off-shore and near-shore wave models, their derivation and appropriate application. It explains why off-shore wave models cannot be used near-shore and why near-shore models are required to obtain accurate wave estimates in shallow water. In this thesis data from off-shore computational models are used as boundary conditions for near-shore computational models. Two near-shore wave models are discussed in chapter 2, SWAN and REF/DIF. While SWAN simulates most near-shore physics well, it has difficulties modelling diffraction (spreading of wave energy), which can be important close to shore. However, it is formulated such that it can be used on a variety of spatial scales. REF/DIF contains a more exact treatment of diffraction, but is limited by computational expense to small areas less than a few hundred square kilometres and cannot simulate wave generation by wind. For this reason SWAN and REF/DIF may be used in a complementary fashion, where SWAN is used at an intermediary between the global-scale off-shore models and the detailed, small scale computations of REF/DIF. When operating SWAN at this medium scale a number of other environmental factors become important, especially wind. Chapter 3 examines the sensitivity of wave estimates from a medium scale SWAN model of the West Coast of Vancouver Island.

The work documented in chapter 3 was performed under the guidance of Michael Tarbotton of Triton Consultants Ltd. as part of a MITACS internship. The purpose was to identify the environmental factors (wind, currents, tidal elevation), modelling options (grid geometry, grid size, solution type) and wave boundary condition resolution (spectral, spatial, temporal) necessary for an accurate and efficient SWAN model of the West Coast of Vancouver Island. The research from this chapter is the most recent and represents a more mature understanding of the complexity to calculating wave conditions.

Chapter 4 presents a case study of the wave climate in Hesquiaht Sound, a small sub region of the medium scale domain investigated in chapter 3. REF/DIF was used for this study because of the presence of a large blocking peninsula and several headlands around which diffraction was thought to be important. The near-shore climate was characterized by propagating the most frequently occurring sea-state offshore of the area for each month. This was done to reduce the number of sea-states to be propagated and provide a realistic snapshot representing a typical sea during any given month. Because wind cannot be accounted when selecting the most frequently occurring seas, and because REF/DIF cannot simulate wave generation by wind, wind was not accounted for and is therefore a limitation of this study.

Chapter 5, the final chapter of this thesis, provides concluding remarks on the presented material, summarizes important contributions and makes recommendations for further work. The framework for near-shore wave climate assessment presented in this thesis may be used by groups or individuals to assess the wave climate in other near-shore regions of the West Coast of Vancouver Island, which may be attractive for WEC deployments. Only with detailed knowledge of the wave climate can we expect commercial extraction to commence.

Chapter 2

A Brief Review of Ocean Wave Models

This chapter discusses selected off-shore and near-shore wave models, their derivation and appropriate application. It explains why off-shore wave models cannot be used near-shore and why near-shore models are required to obtain accurate wave estimates in shallow water. This chapter is important because it provides a discussion of the theory needed to understand the origins of the off-shore wave boundary conditions used in the near-shore computational models of chapters 3 and 4 and the appropriate operation and application of those near-shore models.

2.1 Introduction

Many types of computational wave models exist with typical scales of application ranging from small enclosed harbours to the entire globe. These models can, in general, be classified as either phase-averaging or phase-resolving. Phase-averaging models are expressed as an energy balance with sources and sinks used to account for relevant physical processes. Phase-resolving models are based on the governing equations of fluid mechanics and formulated to solve for the free surface condition. While phase-averaging models have no practical limitation on the size of the area to be modelled, phase-resolving models are currently restricted by computational expense to areas of less than a few hundred square kilometres.

Wave model applicability depends not only on the size of the area to be modelled but also the dominant physical processes affecting wave evolution in that area, including those defined in [1].

1. Wave generation by wind: the development of surface gravity waves caused by the transfer of energy from wind to the ocean surface;

2. Shoaling: an effect whereby wavelength decreases and wave height increases due to a decrease in water depth (as described by the dispersion relationship);

3. Refraction: a turning of wave fronts toward shallower water due to phase speed dependence on water depth. In shallow water, refraction tends to line up wave fronts so that they parallel bathymetric contours;

4. Diffraction: a process which spreads wave energy laterally, orthogonal to the propagation direction, that occurs when waves encounter obstacles whose radius of curvature is comparable to the wavelength of the incident waves;

5. Reflection: a change in direction of a wave front resulting from a collision with a solid obstacle;

6. Bottom friction: a mechanism that transfers energy and momentum from the orbital motion of the water particles to a turbulent boundary layer at the sea bottom;

7. Energy dissipation due to wave breaking: a loss of wave energy due to the turbulent mixing which occurs when wave steepness surpasses a critical level causing water to *spill* off the top of a wave crest;

8. Wave-wave interactions: (triad) two propagating waves exchange energy with a third wave, (quadruplet) four propagating waves exchange energy with one-another;

9. Wave-current interactions: encompasses changes in wave amplitude due to shoaling (caused by current related change in propagation speed), change in frequency due to the Doppler effect and change in direction due to current induced refraction.

Accommodating all of these processes into a single wave model is difficult. Different governing equations and numerical schemes lend themselves to modelling different physical processes and no single model adequately incorporates all of the effects listed above. Off-shore, the dominant physical processes are wave generation by wind, quadruplet wave-wave interactions and a wind induced wave breaking called *white-capping*. Near-shore, the dominant physical processes are refraction, bottom friction, depth induced breaking, triad wave-wave interactions, current-wave interactions and, in very shallow waters, diffraction and reflection [1]. Most wave models target a specific region (e.g off-shore, near-shore, enclosed harbours) and incorporate only the physical processes important in that region. Where a complete modelling solution is required it is common practice to use different models for different regions, applying the results from one model as the boundary conditions to the next.

2.2 Global Wind-Wave Models

Global scale models use wind velocity estimates to calculate wave development and propagation in off-shore climates (the deep oceans). The dominant processes vary slowly and can be adequately resolved using a large grid spacing ($\sim$40km) and a phase-averaging model to handle the required spatial scales. The most extensively used models for wave resource assessment are the British Met Office wave model

(BMOWM) [23], WAM [24] and WaveWatchIII (WW3) [25]. Each of these numerical wind-wave models solves the spectral action density balance equation,

$$\begin{aligned} &\frac{\partial N(t,x,y,\theta,\sigma)}{\partial t} + \frac{\partial C_{g,x} N(t,x,y,\theta,\sigma)}{\partial x} + \frac{\partial C_{g,y} N(t,x,y,\theta,\sigma)}{\partial y} \dots \\ &+ \frac{\partial C_{\theta} N(t,x,y,\theta,\sigma)}{\partial \theta} + \frac{\partial C_{g,\sigma} N(t,x,y,\theta,\sigma)}{\partial \sigma} = \sum_{i=1}^{n} \frac{S_i}{\sigma} \end{aligned} \tag{2.1}$$

where action density is given by:

$$N = \frac{\rho g E(\sigma,\theta)}{\sigma}, \tag{2.2}$$

and where parameters t, x, y, θ and σ are time, the x and y horizontal dimensions, direction, and relative radian frequency respectively. The radian frequency, σ, is relative to the ambient current. Equation (2.1) is an energy balance that includes source/sink terms, S_i, to account for important physical processes. Source terms include: wind input (S_{in}), non-linear wave-wave interaction (S_{nl}), and dissipation (S_{ds}). Though the governing equation is the same for the various off-shore models, each uses a different numerical implementation and utilizes source terms based on different approximations of the wave physics.

WAM and WW3 are considered third generation (3G) wind-wave models due to their fully parametrized handling of wave growth, non-linear wave component interactions and energy dissipation. The BMOWM is considered second generation because it makes *a priori* assumptions in estimating those processes. The BMOWM was used by the British Meteorological Office from the early 1980's until October of 2008 to estimate sea states around the globe. The Met Office is now transitioning to the 3G WW3 model.

WW3 is currently implemented globally by the National Oceanic and Atmospheric

Administration (NOAA), the Fleet Numerical Meteorology and Oceanography Center (FNMOC). NOAA makes forecast and hind-cast model results available via the internet. WAM is used operationally in regional models of the Pacific and Atlantic by Environment Canada (EC) and globally by the European Centre for Medium-Range Weather Forecasts (ECMWF). Forecast data is available from these institutions via the internet but hind-cast data requires special order.

An international effort, coordinated by the ECMWF, to compare results of many operational wind-wave models is reported in [3]. Comparisons were made at the locations of wave measurement buoys. The parameters used to compare the model estimations to the corresponding wave buoy measurements were *bias* (B), *root mean square error* (E_{rms}), *scatter index* (SI) and *correlation coefficient* (r).

In Eqns. (2.3-2.7) below, the subscript $(.)_c$ indicates the model result and $(.)_{obs}$ indicates the buoy measurement, the over-arrow indicates data-set values and the over-bar indicates a mean value. Here the modelled data-set X_c is compared to measured data-set X_{obs} but Eqns. (2.3-2.7) can be used to compare any two data-sets. In this case X, the parameter of interest, represents either H_s or T_p. Error, $\vec{E}$, is the element-wise difference between in the data-sets.

$$\vec{E} = \vec{X}_c - \vec{X}_{obs} \tag{2.3}$$

Bias is the systematic off-set between the data-sets.

$$B = \overline{\vec{E}} = \overline{\vec{X}_c - \vec{X}_{obs}} \tag{2.4}$$

Root-mean-square error is the average absolute difference between the data-sets and is an indicator of model precision.

$$E_{rms} = \sqrt{\overline{(\vec{X}_c - \vec{X}_{obs})^2}} \tag{2.5}$$

Scatter index indicates the relative magnitude of E_{rms} by expressing it as a percentage of the average measured value.

$$SI = E_{rms}/\overline{\vec{X}_{obs}} \cdot 100 \tag{2.6}$$

Correlation coefficient, r, gives the quality of the least squares fit of X_c to X_{obs} (with 1 indicating a perfect fit).

$$r = \frac{\sum(\vec{X}_{obs} - \overline{X}_{obs})(\vec{X}_c - \overline{X}_c)}{(\sum(\vec{X}_{obs} - \overline{X}_{obs}) \cdot \sum(\vec{X}_c - \overline{X}_c))^{1/2}} \tag{2.7}$$

Table 2.1 gives the validation statistics of [3] for the global wave models ECMWF-WAM, BMOWM, FNMOC-WW3 and NOAA-WW3. In Tables 2.1 and 4.2 *Pairs* refers to the number of wave estimates that have corresponding wave measurements. Observing the statistics for H_s, we see that all models show low bias and scatter index and high correlation coefficient, with ECMWF-WAM showing the best results and BMOWM the worst. Observing the statistics for T_p, we see universally poorer performance compared to the H_s statistics. This is largely due to the fact that T_p is an unstable parameter. For T_p, BMOWM again shows the worst performance, but the results from the other models are mixed. NOAA-WW3 has the lowest E_{rms}, SI, and highest r while FNMOC-WW3 has lowest B.

Table 2.1: Verification statistics for global wind-waves model implementations. Table reproduced from [3].

	Model	Pairs	E_{rms}	B	SI	r
H_s (m)	ECMWF-WAM	2456	0.25	-0.02	15.1	0.95
	BMOWM	2456	0.40	0.20	21.0	0.92
	FNMOC-WW3	2456	0.32	0.04	19.2	0.94
	NOAA-WW3	2456	0.33	0.11	18.6	0.94
T_p (s)	ECMWF-WAM	3250	2.18	0.40	26.8	0.63
	BMOWM	3250	3.94	1.65	44.8	0.40
	FNMOC-WW3	3250	2.53	-0.21	31.5	0.54
	NOAA-WW3	3250	2.06	-0.66	24.5	0.65

Evaluated in [3] are several regional models, including EC's East Pacific and North Atlantic models. The H_s bias and scatter index are shown in Table 2.2. Unfortunately, NOAA's WW3 implementation was not included in this comparison. For the Pacific and Atlantic regions, no single model stands out as universally superior, though it is noted that ECMWF-WAM has low B and the lowest SI for both regions.

Table 2.2: Verification statistics for several Pacific and Atlantic regional wind-waves model implementations. Table produced by averaging of Fig. 7 in [3].

		Pacific		Atlantic	
	Model	B	SI	B	SI
	ECMWF-WAM	-0.05	14.5	-0.08	18
H_s (m)	EC-WAM	-0.25	17	-0.06	21
	FNMOC-WW3	0.0	20	-0.16	23

While all models show satisfactory performance, the ECMWF-WAM and NOAA-WW3 have more universally accurate output.

Despite global and regional scale validation, these models may occasionally produce local spurious results due to the presence of unresolved islands or other problematic boundary conditions [26, 27]. Wind-wave model results should therefore be further validated, locally, against available *in-situ* measurements when used as the primary data source for WRA.

2.3 Near-shore Wave Models

Near-shore waves interact significantly with the ocean floor resulting in high spatial variability of the wave field, necessitating small grid spacing (∼50m). Because the size of the area to be modelled is typically less than a few hundred square kilometres both phase-resolving and the phase averaging wave models can be applied near-shore.

Phase-averaging near-shore models, as with global scale models, solve Eq. (2.1), but use additional source terms to account for the most important near-shore transformation processes.

Generally speaking, phase-resolving models can simulate all wave propagation physics, but not the physics of wave development (namely wave generation by wind, whitecapping and wave-wave interactions). Phase-resolving models applied over large areas are depth-integrated such that the governing equation is dependant only on the x and y spatial dimensions. Some of the most widely used phase-resolved models are based on the Mild-Slope Equation (MSE) and the Boussinesq equations. While the MSE is valid for all depths, the Boussinesq equations are invalid in deep water. Since the focus of this work is the propagation of waves from deep water to shallow water, only wave models based on Eq. (2.1) and the MSE will be further investigated.

For a more complete overview of near-shore computational models see [28–30]. Many of the models discussed here and in the mentioned papers have been developed into useful software packages. Two of the most popular packages, SWAN (Simulating WAves Near-shore) [31], and REF/DIF-1 (monochromatic refraction-diffraction) [32] are discussed in the following section.

2.3.1 Near-shore wave modelling software

SWAN, like WW3 and WAM, is a 3G wave model based on Eq. (2.1). Additional physics included in SWAN specific to near-shore modelling are triad wave-wave interactions and depth induced wave breaking. While Eq. (2.1) inherently accounts for refraction it does not account for diffraction. Diffraction in SWAN is accounted for as a spatial smoothing of energy controlled by a diffraction parameter. SWAN uses an implicit numerical scheme. This means that is not subject to the Courant criterion which states that wave energy may not travel more than one grid step in one time step [1]. This allows SWAN to be used at a variety of spatial scales.

REF/DIF-1 is a monochromatic wave model based on the Parabolic MSE (see Section 2.3.2); it inherently accounts for refraction, diffraction, shoaling and forward reflection. The governing equation of REF/DIF is a form of the Parabolic MSE modified to include the effects of wave-current interactions, depth induced breaking and bottom friction. REF/DIF-S, a spectral variant of REF/DIF-1, is essentially equivalent to many concurrent runs of REF/DIF-1; the results are linearly superimposed and a spectral wave breaking model is employed. In the current release of REF/DIF-S only H_s and mean wave direction are available as outputs. For accurate results REF/DIF requires five grid points per wavelength. This restriction limits the applicability of REF/DIF to areas less than a few hundred kilometres.

Both SWAN and REF/DIF have been extensively validated against academic test cases, laboratory experiments and field cases. SWAN validation studies [33, 34] found that it accurately predicts significant wave height with minimal bias and mean period with small (<10%) negative bias. However, both reported significant error in some components of the predicted wave spectrum.

REF/DIF-1 validation studies [35, 36] found that it accurately simulates the processes of refraction, diffraction, shoaling and dissipation, but noted the program does not feature the ability to simulate wave generation by wind. The field test cases given in [35] and [36] were purposely selected for low wind speeds. These studies did not investigate the effect of omitting wave generation by wind on wave field predictions.

The performance of SWAN and REF/DIF-S were compared by [37]. In simulating a laboratory experiment of shoaling and breaking, and a separate experiment of diffraction around a breakwater, both models performed well, but on average SWAN's wave height estimates were more accurate. In simulating a laboratory experiment of refraction and diffraction over a shoal, REF/DIF's wave height estimates were more accurate. The models performed roughly equally for a field case from Duck, North Carolina.

For a broader comparison of near-shore wave propagation software see [38–40][1].

[1] Note the erroneous conclusions in [40] on REF/DIF's ability to predict wave direction as discussed by [41]

2.3.2 REF/DIF-1

REF/DIF-1 is a monochromatic phase-resolving model based on the parabolic approximation to the Elliptic MSE of Berkhoff (1972). Berkhoff's equation is:

$$\nabla \cdot (CC_g \nabla \hat{\phi}) + k^2 CC_g \phi = 0 \tag{2.8}$$

where $C = \omega/k$ and the velocity potential amplitude, ϕ, is related to the velocity potential vector by $\phi = \hat{\phi} e^{-i\omega t}$. The gradient operator operates on only the x and y spatial dimensions due to the depth integration procedure.

The parabolic approximation of [42] reduces the boundary value problem of the Elliptic MSE to an initial value problem. The approximation is made by assuming that waves are propagated primarily in the x-direction and waves reflected in the negative x-direction are neglected. As described in [43] this is realized by assuming

$$\hat{\phi} = -\frac{ig}{\omega} \hat{A}(x,y) e^{i \int k(x,y) dx} \tag{2.9}$$

where $\hat{A}$ is the complex wave amplitude. Substituting Eq. (2.9) into Eq. (2.8) results in

$$\begin{aligned} &\frac{\partial}{\partial x}\left[CC_g \frac{\partial \hat{A}}{\partial x}\right] + 2i(kCC_g)\frac{\partial \hat{A}}{\partial x} + i\frac{\partial (kCC_g)}{\partial x}\hat{A} + ... \\ &\quad \frac{\partial}{\partial y}\left[CC_g \frac{\partial}{\partial y}(\hat{A}(x,y)e^{i\int k(x,y)dx})\right] e^{-i\int k(x,y)dx} = 0 \end{aligned} \tag{2.10}$$

In their derivation of the Parabolic MSE, [44] argue that because waves are assumed to propagate primarily in the x-direction the rate of change of $\hat{A}$ in the x-direction is small. Additionally, when waves encounter an obstacle such as an island or breakwater the slope of the wave in the y-direction may be large in comparison to the x-direction. Following this argument [44] order the derivatives of $\hat{A}$ as follows

$$\frac{\partial \hat{A}}{\partial x} = O(\epsilon^2) \tag{2.11}$$

$$\frac{\partial \hat{A}}{\partial y} = O(\epsilon) \tag{2.12}$$

where ϵ is a small ordering parameter and O is ordering notation. As waves are assumed to propagate primarily in the x-direction, any changes in $\hat{A}$ in the x-direction are primarily due to changes in the water depth. Consequently, derivatives of depth dependant properties are also ordered $O(\epsilon^2)$. Retaining terms to order $O(\epsilon^2)$, only the first term of Eq. (2.10) is lost.

To complete the parabolic approximation, y-direction dependence of wave-number in the integrand is removed. To do this a reference wave-number, $\overline{k}(x)$ is introduced. This is achieved in REF/DIF-1 by averaging wave-number in the y-direction so that the result is only dependant on x [43]. Wave amplitude is then redefined as

$$\hat{A}(x,y) = A(x,y)e^{i(\int \overline{k}(x)dx - \int k(x,y)dx)}. \tag{2.13}$$

Substituting (2.13) into (2.10) and dropping the first term yields the Parabolic MSE.

$$\begin{aligned} 2i(kCC_G)\frac{\partial A}{\partial x} - 2i(kCC_g)(\overline{k} - k)A + ... \\ i\frac{\partial (kCC_g)}{\partial x}A + \frac{\partial}{\partial y}\left(CC_g\frac{\partial A}{\partial y}\right) = 0. \end{aligned} \tag{2.14}$$

The parabolic approximation is limited in applicability to waves which are propagating within approximately 45° of the x-axis. During development of REF/DIF, Kirby and Dalrymple re-derived Eq. (2.14) to include a non-linear correction, to include the effect of currents and to widen the aperture of applicable wave directions to a maximum of about +/-70°. For more on the MSE see [43] and [45]. For more on the governing equations of REF/DIF-1 see [46].

2.4 Summary

The off-shore models BMOWM, WAM, and WW3 are all based on the spectral action density balance equation but each uses a different numerical implementation and source terms which use different approximations to the wave physics. These models are specifically designed for use in the open ocean and do not simulate the complex physics which occur when waves interact with the ocean floor in shallow water. Due to their more advanced handling of wave growth, non-linear wave component interactions and energy dissipation WAM and WW3 tend to be more accurate than the BMOWM. The off-shore wave models discussed here, especially WAM and WW3, can provide excellent spectral wave data appropriate for use as boundary conditions to near-shore models such as SWAN and REF/DIF.

Like the off-shore models, the near-shore wave model SWAN is based on the spectral action density balance equation, but additionally includes triad wave-wave interactions and depth-induced breaking. SWAN handles most near-shore physics, including wave generation by wind very well, but it only approximates diffraction. The implicit numerical scheme used by SWAN allows it to be used over a wide range of spatial scales.

REF/DIF-1 is a near-shore wave model based on the Mild-Slope Equation that inherently models both refraction and diffraction. To ensure accurate results REF/DIF requires at least five grid points per wavelength. Because of computational expense this requirement limits REF/DIF's use to area less than a few hundred square kilometres.

The following chapters use WW3, SWAN and REF/DIF in a complementary manner. Wave data calculated by NOAA's implementation of WW3 are used as boundary conditions to both near-shore models. In chapter 3 SWAN is used at medium scale to estimate wave conditions on the West Coast of Vancouver Island. The results from a medium scale model can be used directly to select promising WEC deployment sites or as boundary conditions to a more detailed model such as the REF/DIF model discussed in chapter 4

Chapter 3

The Effect of Model Set-up on SWAN Wave Estimates

This chapter presents a series of studies which evaluate the sensitivity of a SWAN model of the West Coast of Vancouver Island to environmental factors (wind, currents, tidal elevation), modelling options (grid geometry, grid size, solution type) and wave boundary condition resolution (spectral, spatial, temporal). With such knowledge a model can be constructed using only the necessary inputs. This reduces the cost of building and operating the model, reduces computation time and simplifies trouble-shooting.

The results from a medium scale SWAN model such as the one used in this chapter may be used directly for selecting promising sites for WEC deployment or as boundary conditions to a smaller, more detailed model such as the REF/DIF model discussed in chapter 4.

The work covered in this chapter was performed under the guidance of Michael Tarbotton of Triton Consultants Ltd. during a MITACS Accelerate internship. The work was commissioned in support of the West Coast Wave Collaboration Project, a group committed to the procurement of data and development of computational resources that can be applied in ongoing assessment of the wave energy resource off the West Coast of Vancouver Island, British Columbia (`http://data.axystechnologies.com/smartweb/wcwcp/`).

3.1 Introduction

Simulating WAves Near-shore (SWAN) is a computational model for calculating wave conditions near-shore. The open-source software uses user supplied wave boundary conditions, digital bathymetry and a user-created computational grid to determine the transformation of surface waves in water of arbitrary depth. The model provides spectral descriptions of the waves at discrete locations: the node points of the computational grid. The governing equation of the SWAN model is the discrete spectral action balance equation which is derived from the energy conservation principle. SWAN has been specifically developed for near-shore wave modelling and is normally capable of modelling all the important physical processes that occur as waves approach shore including refraction, diffraction, wave-current interaction and the development of waves due to local winds within the modelled domain. Some of these phenomena are intrinsic to the discrete equations including refraction. Other physical phenomena are incorporated by inclusion of source and sink terms in the governing equation as is the case for wave diffraction effects.

The SWAN model developed in this chapter covers the West Coast of Vancouver Island. Within this area Amphitrite Bank (shown in Fig. 3.1) is of particular interest to many wave energy developers because of the natural focusing of waves that occurs there and the close proximity to shore and electrical grid connection. The West Coast Wave Collaboration Project (WCWCP) has deployed a measurement buoy at this location in an effort to better understand the climate of the area. The testing reported in this work is laying the foundation for the creation of a state of the art

SWAN model, which may be calibrated based on the data recorded by the WCWCP's Amphitrite Buoy.

Typically SWAN is implemented in a stationary mode on a uniform, or regular, computational grid. As the name implies, a uniform grid has a consistent spacing, relative orientation, and density of grid points throughout the modelled domain. While simple to generate, the disadvantage of uniform grids is that the homogeneous grid density must be increased to ensure that accuracy is maintained in the vicinity of small scale bathymetric fluctuations, very shallow water, small islands, etc. Given that the computation time for SWAN executions is directly related to the number of grid points used, the inclusion of fine scale features in the modelled domain often compromises the utility of a uniform computational grid due onerous computation time.

SWAN's "stationary mode" is essentially a steady state analysis of the wave propagation problem. A single off-shore sea-state is specified as a boundary condition and the resulting wave field is calculated throughout the computational grid. Time is not an independent variable in this analysis and consequently the impact of the time varying nature of the climate across the computational grid is neglected. When waves have a long residence time in the modelled domain compared to the time scales of the wind and off-shore wave climate, additional accuracy may be achieved by running SWAN in non-stationary mode. This mode allows seas to be modelled in both space and time allowing, for example, updated wind fields to interact with waves which were generated at the previous time step but are still travelling through the domain. This mode requires time dependent specification of all regular boundary conditions.

Boundary conditions are critical in constructing an accurate SWAN model. In general, time dependent boundary conditions are calculated by using large-scale wind-wave models to hind-cast the wave conditions at off-shore locations. The NOAA WW3 model (discussed in chapter 2) provides detailed spectral data for select locations and parametric summaries are provided for all other locations. FNMOC provides parametric data for both the wind and swell components of the sea. Where detailed spectral wave data is unavailable it can be synthesized from parametric data, but this introduces a large measure of uncertainty into the wave model results. The use of detailed spectral wave data at high spatial resolution along the boundary off a SWAN analysis is uncommon and evaluation of the benefits of using such high resolution boundary conditions would be of great benefit to the wave modelling and wave energy communities.

This chapter evaluates the use of unstructured grids, non-stationary computations, detailed spectral boundary conditions and several more advanced modelling options available in SWAN. Despite best efforts, data availability restricted the current study to examine high fidelity and variable boundary conditions independently. The goal of this chapter is to identify features of SWAN that should be employed in a future wave model of the West Coast of Vancouver Island.

3.2 Methodology

SWAN tests were performed for the West Coast of Vancouver Island between Brooks Peninsula and the Olympic Peninsula with the off-shore boundary straddling the continental shelf. Figure 3.1 shows the bathymetry contours of the domain plotted over a satellite image of the region. It also labels some locations of interest and the white rectangle indicates the domain of the near-shore wave resource assessment of chapter 4.

Several sensitivity studies were used for assessing the relative importance of the various SWAN wave modelling options. In each test a reference model is established and a reference simulation was performed. In subsequent test simulations only a single boundary condition or option was modified. The RMS difference in the wave

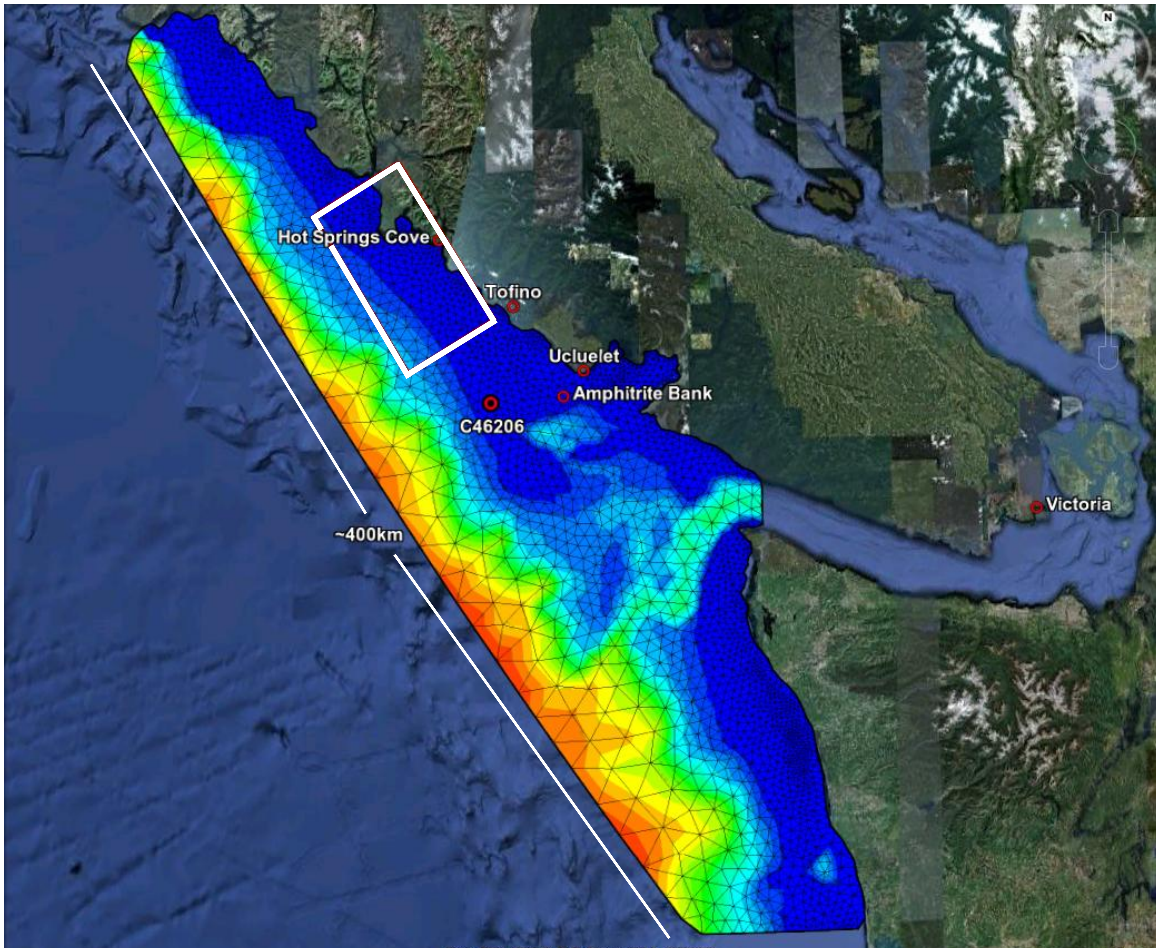

Figure 3.1: Computational domain plotted over satellite imagery of Vancouver Island. Grid *WCVIx1* is shown with colouring representing depth. Sites of interest are labelled. The white rectangle indicates the domain of the near-shore wave resource assessment of chapter 4

parameters significant wave height (H_s), peak period (T_p) and peak direction (θ_p) between the test cases and the reference case were then calculated and used to compare the results. RMS difference is calculated as:

$$E_{RMS}(X) = \sqrt{\sum_i (X_i - X_{Ri})^2/N} \tag{3.1}$$

Where X_{Ri} is the wave parameter value at node i from the reference simulation, and X_i is the wave parameter from the test simulation. N is the total number of nodes.

In each test, unless specified, spectral boundary conditions were constructed using a Pierson-Moskowitz spectrum defined by H_s, T_p and θ_p. Three different wave boundary conditions were repeatedly used in this study. They are indicated as case 1, 2 and 3 in Table 3.1. The $H_s = 3m$, $T_p = 12s$ combination represents some of the largest seas frequently experienced at the off-shore boundary of the region. Approximately 65% of the time H_s is between 2 and 3m. Only 30% of the time is H_s greater than 3m. Wave direction is referenced with zero at due east. The directions of cases 1-3 correspond to the range of θ_p most frequently experienced.

Table 3.1: Wave boundary conditions used in SWAN tests. Directions are reference to due east.

Case	H_s (m)	T_p (sec)	θ_p (°)
1	3	12	0
2	3	12	45
3	3	12	-45

For this work, version 40.72ABCDE of SWAN was used. It was set-up to run with wave breaking, bottom friction, and wave triad calculated using default parameter values. Where wind data was applied, wave quadruplets were calculated using default parameter values. The wave spectrum was discretized into 36 directional bins covering 1-360° and 31 frequency bins covering 0.0521-1Hz. For this work, all other values were left as defaults unless specified.

Bathymetry data covering the computation domain was supplied as an unstructured grid by Triton Consultants LTD. License to the depth sounding from which the grid was derived was obtained from the Canadian Hydrographic Service.

3.3 SWAN Sensitivity Studies

The following sections present qualitative information gathered during the preparation, execution and post processing of SWAN simulations, as well as quantitative data assessing the impact of varying simulation parameters. While none of these tests are exhaustive and all are specific to the selected geographic region, conservative conditions were assigned in the reference cases to ensure that the results give clear and unbiased indications of each options significance. The presented results are intended to guide the construction of future SWAN models for other similar sized domains. Application of these results to other regions should be done with care. The commonly experienced wave, wind, current and tidal range conditions in a region will influence the importance of each of the modelling options. Ideally, a similar study would be performed prior to establishing a SWAN prediction model in any region.

3.3.1 Computations on unstructured grids

The use of unstructured grids allows both good representation of shorelines and continuously variable grid resolution throughout the modelled domain. In this way nodes can be allocated to the areas which require high grid resolution, without requiring that high grid resolution be applied to the entire domain. SWAN has recently added the option to perform computations on unstructured grids. Computations on unstructured grids in SWAN may be performed on multiple CPU cores but, as of version 40.72ABCDE, the option to include diffraction effects is not available for unstructured computations.

Using unstructured grids with SWAN significantly reduces the number of nodes needed to obtain accurate results for most problems but the number of nodes is still limited by the hardware of the computer being used. A rough estimation of the maximum number of grid points that can be used is:

$$\text{max nodes} = \text{internal memory (in bytes)} / (4 \text{ x } \# \text{ of spectral bins})$$

In modelling complex shorelines it may be convenient to eliminate some inlets, bays and estuaries which are not of interest from the computational domain. This should be done with caution; while SWAN does allow for an open boundary condition through which waves can pass unimpeded, the numerical condition does not always work perfectly and erroneous wave estimates may be experienced near the boundary. Where possible, open boundary conditions should not be located near a particular area of interest. See the SWAN user manual [47] (page 11) for more details.

Unstructured grid generation

Unlike most unstructured ocean models, SWAN uses finite difference computations rather than finite element. Most unstructured mesh generators are designed for finite element computations, which do not explicitly calculate derivatives from nodal values. One such grid generator is TriGrid [48]. Originally developed at the Institute of Ocean Sciences for tidal flow modelling, TriGrid has had many contributors including R.F. Henry, Scott Sloan, Triton Consultants LTD., R.A. Walters, Channel Consulting LTD. and A.G. Dolling. TriGrid, along with its manual grid modification features, was found to produce grids satisfactory for use in SWAN.

As a basic requirement, SWAN specifies that each internal node must be connected to between four and ten neighbouring nodes. Problems may be encountered at locations where a boundary node is connected to more than two other boundary nodes. At locations 'A' and 'D' in Fig. 3.2 the outer (main) boundary of the domain is connected directly to an internal (island) boundary. Since the wave energy is dissipated at shore, the wave energy is nominally zero at boundary nodes. With no connection to internal nodes, SWAN cannot propagate wave energy into the channel. At location 'B' and 'C' nodes from the main boundary bridge the inlet and are directly connected to nodes on the other side of the inlet. SWAN interprets this as multiple boundaries and may terminate the simulation. In TriGrid, boundary anomalies must be identified and removed manually.

Special attention must be given to the grid quality in regions where the bathymetry

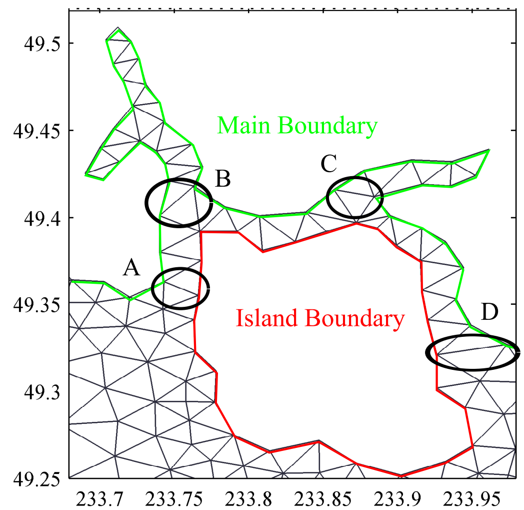

Figure 3.2: A grid of the region around Flores Island, BC. This grid is too coarse to adequately model the propagation of waves into the narrow inlets surrounding the island. Problem areas are indicated at A-D.

changes very rapidly such as around sea-mounts or sub-sea canyons. The natural focusing effect that may be observed around these features may be numerically magnified if the focal region is not adequately resolved. TriGrid can produce meshes with element size proportional to depth, but not proportional to the gradient of depth. This would be a useful feature to include to make TriGrid more applicable to wave modelling. For this work, several of these troublesome regions were identified during preliminary model runs, including Destruction Island, Washington. The grid resolution around these areas was increased by manual manipulation of the grid in TriGrid. Though finicky, and impractical for very large meshes, manual mesh manipulation is a very valuable tool when portions of an automatically generated mesh are unsatisfactory.

Mesh resolution

It is expected that the accuracy of SWAN results is dependant on the resolution of the bathymetric grid used. A study was performed to assess the sensitivity of wave estimates to the distance between computational nodes, *grid dimension* d_x. An initial grid, *WCVIx1* was constructed using TriGrid. The element areas were constructed proportional to the local water depth which was provided by a *depth grid*. *WCVIx1* was subdivided three times to create three additional grids of increasing resolution. The subdivision process places an additional node at the mid-point of every node connection. The nodes are then re-triangulated to create new node connections. Each grid subdivision approximately quadruples the number of nodes. During re-triangulation some nodes may be deleted in order to maintain grid quality requirements.

Table 3.2 gives the number of nodes, maximum and minimum d_x and the average ratio of grid dimension to water depth for each grid. Water depth is indicated by h. Grid dimension was calculated as the average length of all the element sides connecting at the node. The minimum grid dimension in the *WXCIx4* grid is longer than in the *WXCIx3* grid. This is because the smallest element in the *WXCIx3* grid was eliminated during re-triangulation of the *WXCIx4* grid.

Table 3.2: Grids used in mesh resolution study.

Grid name	Nodes	max. d_x (m)	min. d_x (m)	ave. d_x/h (m/m)
Dep. grid	N/A	18369	235	20.5
WCVIx1	2580	16902	533	49.3
WCVIx2	9945	8451	76.7	24.7
WCVIx3	39010	4226	38.4	12.4
WCVIx4	154498	2113	53.2	6.2

The performance of each grid was assessed by comparing its results to the highest resolution grid, *WCVIx4*. The root-mean-square difference in H_s, T_p, and θ_p between the grids *WCVIx1-3* and *WCVIx4* are given in Table 3.3 for cases 1-3. The RMS difference in H_s is shown in Fig. 3.3 for cases 1-3. For all cases, reduction in RMS difference in wave parameters with increasing grid resolution was observed.

Figure 3.4 gives the frequency distribution of grid dimension for each grid. A bin-

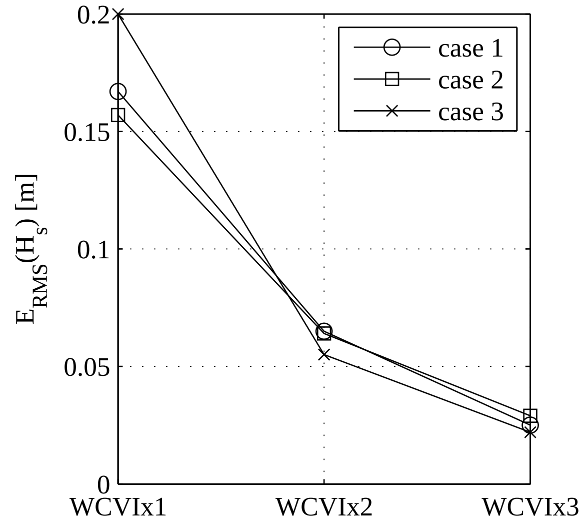

Figure 3.3: Convergence of RMS difference of SWAN solution with grid resolution.

width of 200m was used. As grid resolution is increased a greater proportion of nodes are pushed towards the lower-end of the grid dimension spectrum. In the author's opinion *WCVIx2* provides the best trade-off between resolution (computation time) and wave estimate accuracy. It is notable that the averaged ratio of grid dimension to water depth (d_x/h) for *WCVIx2* is closest to that of the *depth grid*. This suggest that model grid resolution should be close to that of the source depth grid, as is typically suggested for hydro-kinetic ocean models.

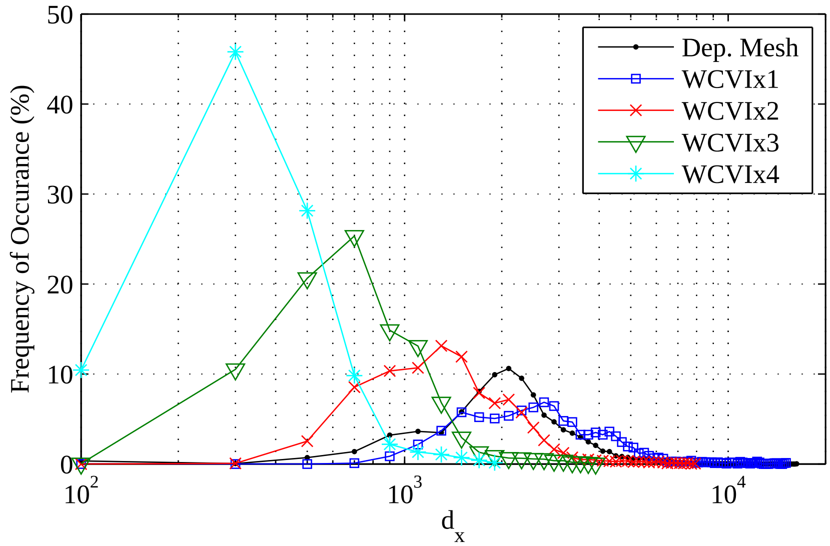

Figure 3.4: Histogram of mesh element sizes for each mesh. Bin-width = 200m

Table 3.3: Mesh performance compared to the highest resolution mesh, *WCVIx4*

Mesh name	$E_{RMS}(H_s)$	$E_{RMS}(T_p)$	$E_{RMS}(\theta_p)$
Boundary conditions: H_s=3m, T_p=12s, θ_p=0°			
WCVIx1	0.167	0.357	11.6
WCVIx2	0.065	0.29	6.8
WCVIx3	0.025	0.24	4.1
Boundary conditions: H_s=3m, T_p=12s, θ_p=45°			
WCVIx1	0.157	0.33	11.0
WCVIx2	0.064	0.23	6.3
WCVIx3	0.029	0.16	4.6
Boundary conditions: H_s=3m, T_p=12s, θ_p=-45°			
WCVIx1	0.20	0.55	13.5
WCVIx2	0.055	0.37	7.57
WCVIx3	0.022	0.24	4.65

3.3.2 Wave generation by wind

SWAN has the ability to simulate wave generation by wind. To study the influence of wind on wave estimates a sensitivity study was performed. For this study and the remainder of the studies in this chapter, computational grid *WCVIx2* was used. Boundary conditions were constructed using a Pierson-Moskowitz spectrum defined by H_s, T_p and θ_p. To assess the influence of the wind on the wave field, the same wave boundary conditions were used for various wind speeds and directions. Winds were applied uniformly over the domain. Wind speeds of up to 20m/s were applied. Wind speeds up to 20m/s are observed regularly by the La Perouse Wave Buoy. Figure 3.5 shows the wind speed duration curve for measurements taken from the Buoy. Shown below in Table 3.4 are the RMS differences between wave simulations with and without wind included.

Table 3.4: The difference between simulations of various wind speed and direction as compared to a simulation without applied winds.

$\lvert v_{wind} \rvert$ (m/s)	θ_{wind} (°)	$E_{RMS}(H_s)$	$E_{RMS}(T_p)$	$E_{RMS}(\theta_p)$
Boundary conditions: H_s=3m, T_p=12s, θ_p=45°				
1	0	0.023	0.13	2.8
5	0	0.078	0.40	4.
10	0	0.517	0.59	9.1
20	0	2.37	3.10	35.7
5	180	0.082	0.35	6.8
10	180	0.447	0.54	9.0
Boundary conditions: H_s=3m, T_p=12s, θ_p=0°				
20	0	2.61	2.76	13.7

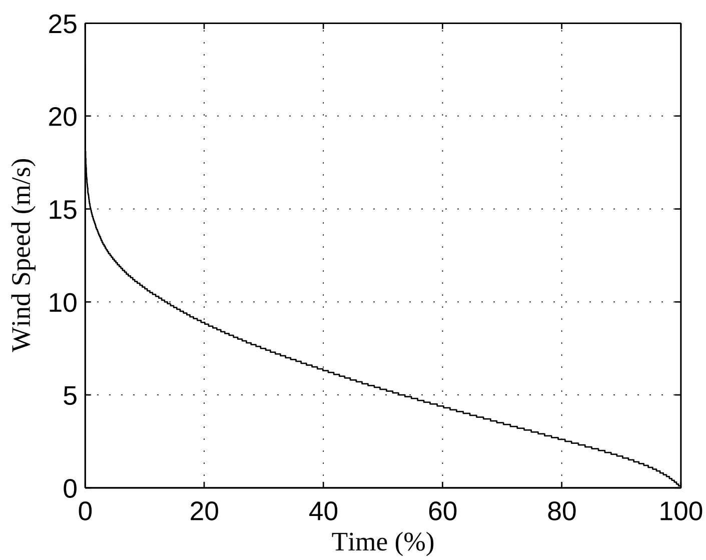

Figure 3.5: Wind speed duration curve for measurements taken by the La Perouse Buoy (1988-2010).

Table 3.4 shows significant increase in H_s for wind speeds over 5m/s. Figure 3.5 shows that approximately 50% of the time wind speed is greater than 5m/s. It is worth noting that the wave boundary conditions are not representative of fully developed wave conditions for the given wind speed. This is equivelent to fully developed waves encountering a wind system near-shore which is different than the wind system which generated the waves.

To evaluate the influence of local winds similar to those which generated the off-shore wave boundary conditions, the off-shore waves were specified to correspond to the applied wind field. For deep water, H_s and T_e for fully developed seas can be estimated based on wind speed [49] using Eqns. (3.2) and (3.3). Here, for simplicity, T_p is assumed equal to T_e.

$$H_s = 2.482 \cdot 10^{-2} U_{10}^2 \tag{3.2}$$

$$T_e = 8.30 \cdot 10^{-1} U_{10} \tag{3.3}$$

Here U_{10} is the wind speed at 10m altitude. Three simulations were run with wind speeds from 5 to 20m/s. The results are given in Table 3.5.

Table 3.5: The difference between simulations of various wind speed and direction as compared to a simulation without applied winds. Boundary conditions were selected to correspond to fully developed seas based on the applied wind condition.

$\lvert v_{wind} \rvert$ (m/s)	θ_{wind} (°)	$E_{RMS}(H_s)$	$E_{RMS}(T_p)$	$E_{RMS}(\theta_p)$
Boundary conditions: H_s=0.621m, T_p=4.15s, θ_p=0°				
5	0	0.10	0.43	8.0
Boundary conditions: H_s=2.482m, T_p=8.30s, θ_p=0°				
10	0	0.35	0.55	7.1
Boundary conditions: H_s=5.585m, T_p=12.45s, θ_p=0°				
15	0	0.80	0.82	7.5
Boundary conditions: H_s=9.928m, T_p=16.60s, θ_p=0°				
20	0	1.39	1.41	8.02

The differences shown in Table 3.5, though less than in the in Table 3.4, are still significant. The differences are less because the seas are already at a fully developed state when the simulation starts, so it is expected that any further energy added to the sea by the wind will be dissipated by white capping. The situation is actually more complex, because as the waves propagate toward the irregular coastline wave height diminishes due to refraction and bottom friction. Where wave height is diminished from the boundary condition value, local winds have the opportunity to add energy back to the sea.

These finding show that in a domain as large as the one in the present study, local winds must be included to obtain accurate wave estimates, but the question remains how spatially resolved the input needs to be.

Resolved wind field

This section assess importance of the spatial resolution of the wind fields used in SWAN. Ten metre elevation wind data from the Coupled Ocean Atmosphere Mesoscale Prediction System (COAMPS) is available through `www.usgodae.org` for the eastern Pacific at a resolution of 0.2°x0.2° (approx 14x11km). This data, for 2010-08-03 12:00, was interpolated onto grid *WCVIx2* and input to a SWAN simulation with case 2 wave boundary conditions.

For comparison, an additional SWAN run using case 2 boundary conditions and a constant wind boundary condition ($|v_{wind}|$=2.91m/s, θ_{wind}=5°) was taken from 48.83°N,126°W of the COAMPS dataset. The location 48.83°N,126°W is that of the La Perouse buoy. In addition, the same wave boundary conditions were again used, but this time no wind conditions were applied. The RMS difference between the no-wind, the constant wind, and the variable wind simulations are given in the Table 3.6 below.

It is notable that $E_{RMS}(H_s)$ with constant wind is almost as large as with no wind at all. Little difference is seen in T_p and θ_p, but the wind velocity is quite low. To further investigate the influence of using resolved wind data, the same process as

Table 3.6: The influence of wind spatial variability on wave estimates

$\lvert v_{wind}\rvert$ (m/s)	θ_{wind} (°)	$E_{RMS}(H_s)$	$E_{RMS}(T_p)$	$E_{RMS}(\theta_p)$
Case 2 boundary conditions: H_s=3m, T_p=12s, θ_p=45°				
0	0	0.072	0.13	3.1
2.91	5	0.049	0.15	3.2

above was used for a day with greater winds, 2010-01-25 12:00. Table 3.7 shows the RMS differences of the simulations with constant wind (again from 48.83°,-126°) and no-wind simulations as compared to the simulations with resolved wind input.

Table 3.7: The influence of wind spatial variability on wave estimates

$\lvert v_{wind}\rvert$ (m/s)	θ_{wind} (°)	$E_{RMS}(H_s)$	$E_{RMS}(T_p)$	$E_{RMS}(\theta_p)$
Case 2 boundary conditions: H_s=3m, T_p=12s, θ_p=45°				
0	0	1.57	2.09	48.7
17.6	125.7	0.51	1.51	15.1

The RMS differences between the case with no wind and the case with variable wind are very large. Not accounting for wave growth due to wind in this case would result in a wave height estimate errors of 1.5m. The constant wind case is a better approximation, but still the RMS error in wave height is 0.5m. For modelling the West Coast of Vancouver Island it appears very important to account for wind in the most detailed manner possible.

3.3.3 Wave-current interactions

SWAN has the ability to calculate wave transformation and propagation in the presence of currents. A test was performed to assess the influence of currents on wave estimates. For each test the Case 2 wave boundary conditions were used and a number of current speeds and directions are applied uniformly over the computational domain. WebTide [50], a two-dimensional, harmonic tidal model was used to estimate tide-driven current velocity around Amphitrite Bank. A maximum speed of approximately 0.3m/s was found. Experimentation with the model showed that current magnitudes tended to diminish further from shore. As a conservative measure, current speeds of up to 2m/s were applied, which is nearly ten times the predicted current speed in the area of interest . The results are given in Table 3.8.

Table 3.8 shows that a current of 1m/s has relatively little influence on wave estimates. The maximum RMS difference in H_s is when the current is flowing at 45° to the x-axis at which it is in-line with the wave propagation direction. At 2m/s the current does cause significant differences in all parameters, but is much higher than current speed predicted for this area.

Table 3.8: The influence of current speed and direction on wave estimates

$\lvert v_{cur}\rvert$ (m/s)	θ_{cur} (°)	$E_{RMS}(H_s)$	$E_{RMS}(T_p)$	$E_{RMS}(\theta_p)$
Boundary conditions: H_s=3m, T_p=12s, θ_p=45°				
1	0	0.046	0.42	5.6
1	45	0.111	0.83	7.9
1	90	0.060	0.44	6.5
1	180	0.055	0.47	5.7
1	270	0.065	0.46	6.9
2	45	0.206	1.77	21.7

The present study has not assessed the influence of geographically variable currents or the geographic resolution of the current data. A separate circulation model would be required to produce the necessary current field data. Additionally, the influence of currents on wave power transport has not been assessed. These topics require further investigation and are left for future work. Though in this particular case currents were found to not significantly influence wave height transformation, it may be important in other higher velocity environments as has been found in studies in the Bay of Fundy.

3.3.4 Change in water level due to tides

The SWAN user manual suggests that changes in water level can have a large effect on wave estimates. To test the validity of this hypothesis over the full spectra of physical conditions inside the SWAN grid, six different simulations were run, each with the same boundary conditions but with different tidal off-set (Δh). The RMS differences between the run with zero off-set and the runs with negative off-set are given in Table 3.9 below. Table 3.9 show a significant increase in $E_{RMS}(H_s)$ with Δh. Predictions made using WebTide [50] for the area near Ucluelet show that water level differences of 1.5m are seen regularly. A Δh of -1.5m corresponds to approximately $E_{RMS}(H_s)$=11cm. It should be noted that most of this difference is in the surf zone as shown in Fig.3.6.

Unless wave estimates in the vicinity of the surf zone are of particular interest, accounting for changes in water level due to tides is likely unnecessary.

Table 3.9: The influence of water level on wave estimates

Δh (m)	$E_{RMS}(H_s)$	$E_{RMS}(T_p)$	$E_{RMS}(\theta_p)$
Boundary conditions: H_s=3m, T_p=12s, θ_p=0°			
-1	0.071	0.13	4.5
-2	0.146	0.17	6.1
-3	0.206	0.21	7.7
-4	0.256	0.25	9.1
-5	0.282	0.28	10.0

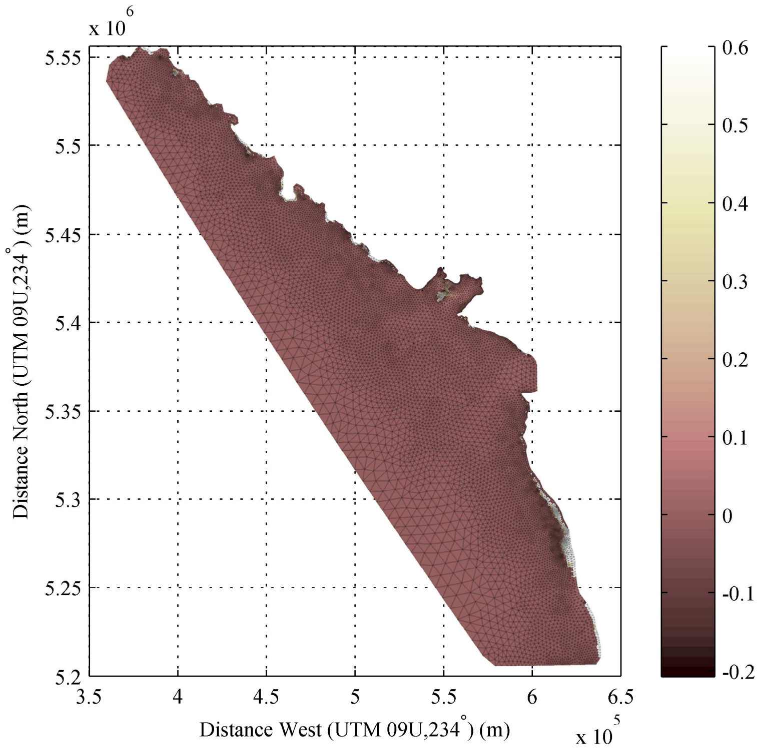

Figure 3.6: The difference between H_s estimates with Δh=0m and Δh=-2m.

3.3.5 Non-stationary computations

Wave conditions can only be approximated as stationary over a sufficiently short expanse of time and space. Typically SWAN is run in stationary mode, where a single steady-state solution is sought. Non-stationary computations add time as an independent variable to the wave propagation problem, requiring multiple boundary conditions and yielding multiple solutions (one for each time-step). Performing non-stationary simulations better emulates the real, time-varying nature of the environment but, the requirement for multiple boundary conditions makes them more difficult to set-up and the result of multiple solutions makes them more difficult to analyse.

Stationary simulations lend themselves to convergence analysis because a single is produced. But, because stationary computations require iteration to achieve a converged solution, they are less computationally efficient than non-stationary computations. The multiple solutions yielded by non-stationary simulations introduces vagarity in the choice of solution used for convergence checking. In SWAN non-stationary computations can be executed with user supplied initial conditions (*hot-start*) or without initial conditions (*cold-start*), in which case SWAN estimates the initial conditions based on the wave and wind boundary conditions.

Cold Start

As a rough comparison of stationary and non-stationary computations, a *cold-start* non-stationary simulation was run for 79 simulated hours with case 1 boundary conditions applied at each time step. The results of this simulation were compared to a stationary computation with case 1 boundary conditions.

Figure 3.7 shows the convergence of parameters H_s, T_p, θ_p to the stationary solution. Initially the RMS differences in all parameters is large; this is due to inaccuracy in the initial conditions assumed by SWAN. Since SWAN estimates the initial wave height from the local winds, it is not surprising that in a simulation run without applied winds that the initial estimates of H_s are inaccurate. It takes about 35 simulated hours for the initial waves to propagate through the domain and dissipate at shore. The error in T_p is initially large, but diminishes in about ten hours. This indicates that SWAN's initial estimate of T_p is quite good except for areas close to shore. Error in θ_p degrades at a rate similar to H_s, suggesting that SWAN's initial estimate is uniformly inaccurate throughout the domain.

After 79 simulated hours the RMS difference between the stationary and non-stationary computations were negligible: $E_{RMS}(H_s) = 0.0035$, $E_{RMS}(T_p) = 0.0483$, $E_{RMS}(\theta_p) = 0.5014$. The final difference in the results of the two modes is likely dependant on both the stopping criteria (the condition which specifies when the solution is considered 'converged') for the stationary computation and the number of time periods the non-stationary computation is run for.

Hot Start

To evaluate the importance of user-supplied initial conditions, a *hot-start* non-stationary computation was made using initial conditions sourced from a stationary computation with boundary conditions: H_s=2.9m, T_p=9s, θ_p=30°. These boundary conditions were selected as a plausible preceding sea-state to our base case of: H_s=3m, T_p=12s, θ_p=0°. Observing Fig. 3.7 it is apparent that H_s converges much faster when initial conditions are provided. T_p on the other hand converges slower, because in this scenario the entire domain is filled with spectra calculated from the boundary conditions of the previous time-step in which T_p is 30° different from the current one. θ_p exhibits similar behaviour as H_s and θ_p in the cold-start, with ∼35 hours required to propagate out the initial differences.

This 35 hour residence time shows the importance of using non-stationary computations for a domain of this size. Stationary computations may not be accurate even when the sea conditions are changing relatively slowly. That is, for a given off-shore boundary condition, the stationary solution may never be achieved in the time that the boundary condition is valid.

Non-stationary computations are the standard for global wave model implementations such as the WW3 models run by NOAA and FNMOC, but stationary simulations are more often used for near-shore analysis. This section has shown that, at least for medium sized domains, stationary simulations may not capture the true nature of the wave climate and, where possible non-stationary simulations should be used. Since the discrepancy in wave estimates arises from the residence time of waves in the domain, it is reasonable to assume that the importance of non-stationary computations is linearly related to the shore-ward extent of the domain.

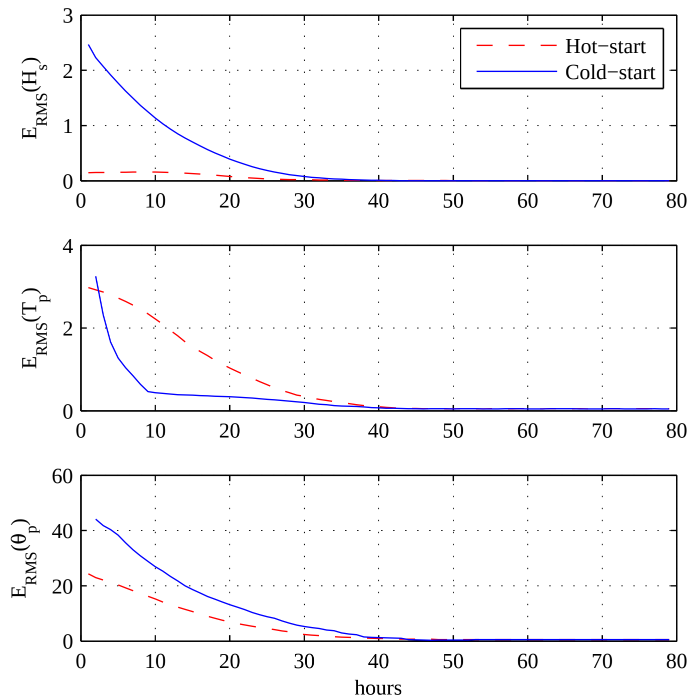

Figure 3.7: Difference between non-stationary (hot and cold start) and stationary solutions through modelled time. Case 1 boundary conditions are used for both computations. For the hot-start, initial conditions were taken as the results to a previous stationary simulation with boundary conditions: H_s=2.9m, T_p=9s, θ_p=30°. For the cold-start, initial conditions were estimated by SWAN (based on boundary conditions and wind conditions).

3.3.6 Variable boundary Conditions

Observing Fig. 3.1 it seems only reasonable that the wave conditions along the outer boundary of the computational domain are variable - the outer boundary spans nearly 400 km. Examining eight years of data from NOAA's Alaskan Waters WW3 model at 47°N125°W, 48°N126°W, 49°N127°W and 50°N128°W (indicated in Fig. 3.8), it was found that the boundary is in fact variable. The mean standard deviation of H_s, T_p, and θ_p was 0.22m 0.84s and 12° respectively.

Data from FNMOC's Global WW3 on 12:00pm on 2010-07-01 was used to assess the influence of variable boundary conditions on wave estimates in SWAN. A simulation was performed with boundary conditions as specified in Fig. 3.8 and interpolated between the specified points. The results were compared to a simulation using a constant boundary condition of H_s=0.89m, T_p=8s, θ_p=347°. The differences between the simulation with variable and constant boundary conditions was: $E_{RMS}(H_s) = 0.139m$, $E_{RMS}(T_p) = 2.72s$, $E_{RMS}(\theta_p) = 49°$. These results show that even though there was not significant variation of H_s along the outer boundary, the differences in T_p and θ_p significantly affected the wave estimates.

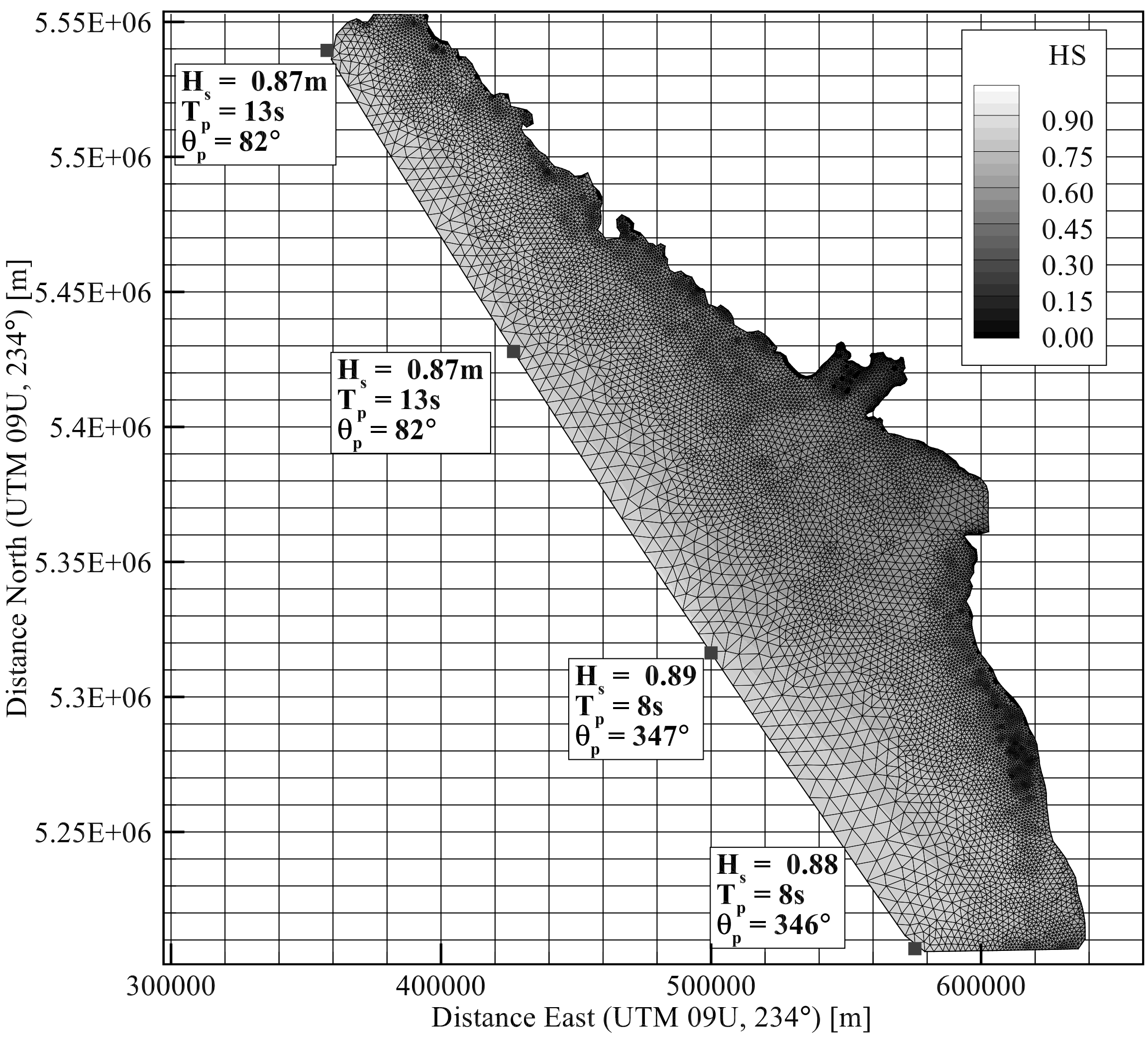

Figure 3.8: Computational domain, boundary condition, grid and H_s estimate for case study of variable boundary conditions. Boundary conditions obtained from FNMOC Global WW3 wave model. Boundary conditions constructed based on H_s, T_p, θ_p using Pierson-Moskowitz spectrum and are interpolated by SWAN between the specified points.

3.3.7 Fully-defined spectral boundary conditions

Typically SWAN constructs spectral boundary conditions based on the parameters H_s, T_p, θ_p using a Pierson-Moskowitz or other synthetic spectrum. SWAN has the ability to use user-defined spectra as boundary conditions. These spectra could come from measurement equipment or other computational models. A spectrum computed by the NOAA WW3 Alaskan Waters model at point 46206 (shown in Fig. 3.1) for 12:00am of 2009-07-13 was transplanted to the boundary of the SWAN model for comparison of wave estimates with and without fully defined spectral boundary conditions. Though this spectrum does not accurately represent the wave conditions at the SWAN outer boundary, it was the closest available spectral data. For this spectrum H_s=1.09m, T_p=4.8s, θ_p=346°. The SWAN simulation used for comparison was calculated using boundary conditions based on a Pierson-Moskowitz spectrum formed around this set of parameters. The fully-defined directional variance density spectrum from point 46206 is given in Fig. 3.9. There are several components to the spectrum shown in Fig. 3.9, from multiple swell components and from waves generated by local winds. Because the spectrum contains several peaks it is expected that the simulation utilizing this fully-defined spectrum will produce substantially different results than the simulation utilizing the Pierson-Moskowitz approximation.

The RMS difference between the simulation with fully-defined spectral boundary conditions and the simulation with the parametrically defined boundary conditions were: $E_{RMS}(H_s) = 0.218m$, $E_{RMS}(T_p) = 3.81s$, $E_{RMS}(\theta_p) = 8°$. These results show that spectral shape can have a significant influence on wave estimates.

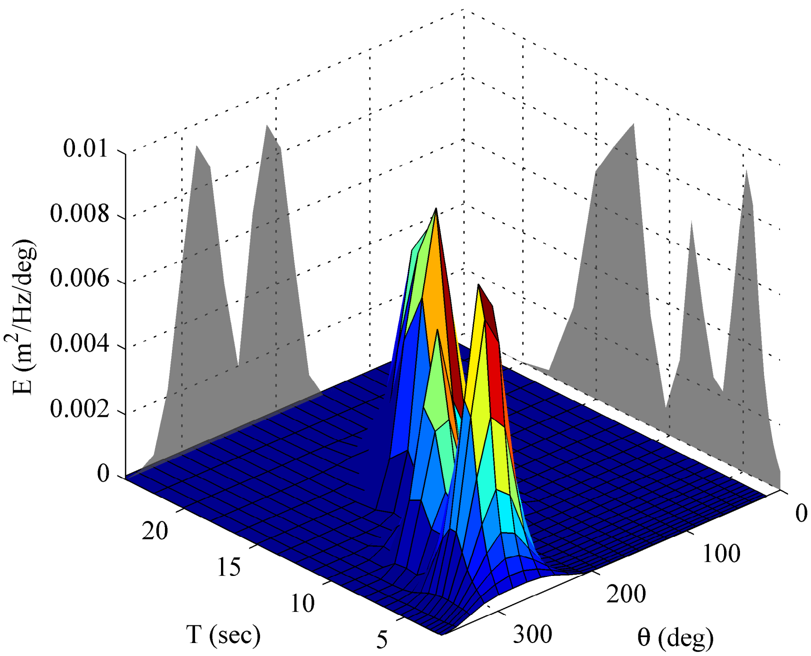

Figure 3.9: Variance density spectrum used in study of fully defined wave spectral boundary conditions in SWAN. T is period corresponding to each bin of the spectrum.

3.3.8 Quality of FNMOC parametric spectra

In many cases, full directional spectra suitable for use as boundary conditions in SWAN are not available. The most common boundary data is parametric: H_s, T_p and θ_p.

Storing historical archives of full spectra is memory intensive. As a compromise some institutions store parametric data for several components of the spectra, typically the swell sea and the wind sea. FNMOC stores H_s, mean period and direction parameters T_e and θ_e for the swell and wind sea and H_s, T_p and θ_p for the overall spectrum.

This section examines the accuracy of synthesising wave spectra from FNMOC parametric data. Spectra synthesised from parametric data are compared to modelled or measured spectra. The RMS difference method used in the other studies in this chapter was not used here because the results would be dependant on the magnitude of the energy in the spectrum, instead Deviation Index is used. First proposed in [51], Deviation Index (DI) is the weighted sum of the percentage difference of each component in the spectra. Though DI is the sum of percentages, it is not percentage error, and therefore may be greater than 100%.

$$DI = \sum_{i=1}^{N-1} \left[\left(100 \frac{|S^*(f_i) - S(f_i)|}{S^*(f_i)} \right) \left(\frac{S^*(f_i)\Delta f_i}{m_0} \right) \right] \tag{3.4}$$

Deviation Index has been modified here for directional spectra to include error in the direction dimension. Because the directional error is included, results from Eqns.(3.4) and (3.5) cannot be compared directly.

$$DI = \sum_{j=1}^{M-1} \sum_{i=1}^{N-1} \left[\left(100 \frac{|S^*(f_i,\theta_j) - S(f_i,\theta_j)|}{S^*(f_i,\theta_j)} \right) \left(\frac{S^*(f_i,\theta_j)\Delta f_i \Delta\theta_i}{m_0} \right) \right] \tag{3.5}$$

The location used for comparison, 46.1N 131.001W, was selected because FNMOC parametric data, NOAA WW3 directional spectral data and NDBC buoy-measured non-directional spectral data are all available very close to this point. One and two peaked directional spectra were created from FNMOC parametric data for comparison to the directional spectra from the NOAA's WW3 model. One and two peaked non-directional spectra were created from FNMOC parametric data for comparison to the non-directional spectra measured by NDBC buoy 46005. The synthetic two peak non-directional spectra were created by superposition of two Pierson Moskowitz spectra. Directionality was added using cos^2 directional spreading for each peak. More advanced functions for spectral shape and directional spreading exist, but require more information than was available.

For the directional spectra, twelve different seas were compared for the year of 2006, each from 12:00 UTC on the first day of the month. Figure 3.10 gives DI for each of the spectra. It shows that in many cases the 1-peak synthetic spectra give lower DI than the 2-peak. It is believed this is because mean values of period and direction are used to create the two peak spectrum. If there are several swell peaks, the mean parameters T_e and θ_e will locate a single swell peak somewhere between the two, perhaps missing them both entirely. On the other hand the single peak spectra is located by T_p and θ_p, which correspond to the largest peak in the spectrum.

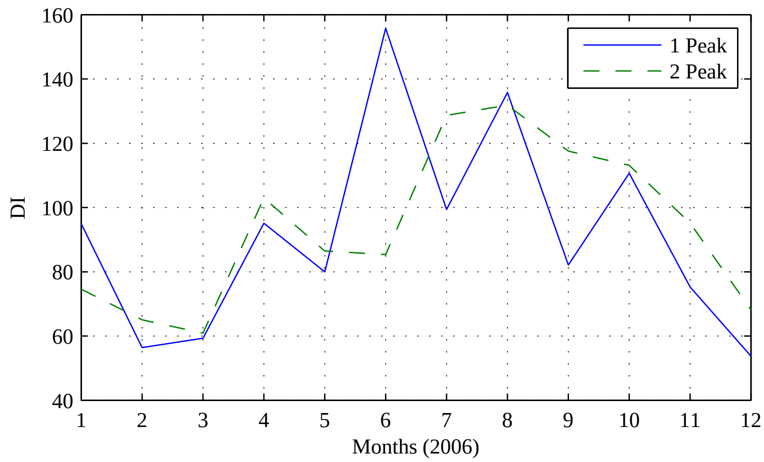

Figure 3.10: Deviation Index of directional 1 and 2 peak parametric spectrum as compared to NOAA WW3 directional spectrum.

Because of limited buoy data, only eight non-directional spectra were compared. Overall, DI is lower than for directional spectra because error in direction is not included. Compared to the optimized fits (DI=11-66) obtained in [52], the DI found here is substantially higher. [52] used spectral shape and directional spreading functions of higher order than what is utilised here and used optimization to find the values of the additional parameters which gave the best fit to the original directional spectrum. They also had access to the spectra from which they derived the parametric data. In the current case the parametric data from one wind-wave model is being fit to the spectra from another model. There is no guarantee that the spectra from which the FNMOC parametric data was derived correlates to either the NOAA WW3 spectra or the spectra measured by buoy 46005. Given the circumstances, the

DI found for the non-directional spectra are satisfactory.

In this case the DI for the 2-peak spectra is as low or lower than the 1-peak for all months except December. This suggests that the larger DI in the 2-peak directional spectra may be due mostly to errors in direction, but alternatively it may mean that the FNMOC parametric data has greater correlation to the spectra measured by buoy 46005 than the spectra modelled by the NOAA's WW3 model.

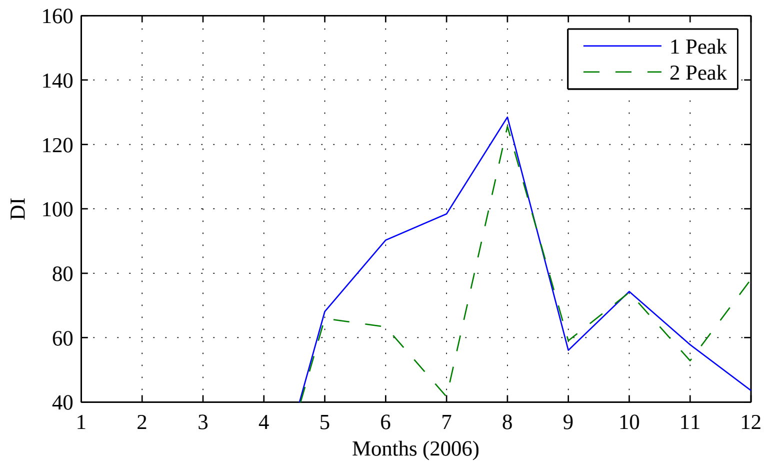

Figure 3.11: Deviation Index of non-directional 1 and 2 peak parametric spectrum as compared to measured spectra from NDBC buoy 46005.

3.4 Summary

This chapter has presented findings on the importance of using various options of the wave model SWAN for accurate prediction of wave conditions on the West Coast of Vancouver Island.

It was found that wave estimates could successfully be performed on unstructured computational grids. For this case it appears that a grid resolution similar to the resolution of the available bathymetry is most appropriate. Though unstructured grids may reduce computation time, and in some cases increase accuracy, care must be exercised in their construction. Small inlets, islands and other locations with very irregular boundaries can cause anomalies which results in errors in wave estimates or execution errors. Additionally, locations with abrupt changes in local bathymetry require special attention, as natural focusing effects can be numerically magnified if the area is not adequately resolved.

Applied winds were found to have a very large impact on wave estimates. The resolution of the wind data was also found to have a significant impact on wave estimates. It is recommended that wind fields be applied to the model in the most detailed manner possible.

The tidal currents normally experienced in this region did not have a significant impact on wave estimates. Uniform current fields were used for the study. The impact of geographic variability and geographic resolution of the current field on wave estimates were not assessed. The influence of change in water level due to tides was also investigated and was found to have little influence on wave estimates except in the surf zone.

Non-stationary SWAN computations were found to yield the same results as stationary computations when given identical boundary conditions. Given the long wave residence time for a domain of this size non-stationary computations are expected to provide the most accurate results with the least computational expense.

Both the spatial and the spectral resolution of the wave boundary conditions were found to significantly affect wave estimates within the domain. The most detailed wave boundary conditions available should be used.

Based on limited data available, it appears that synthesising directional spectra from FNMOC swell-wind parametric data gives a relatively poor approximation of the real wave spectrum. Thus far, FNMOC parametric data has been compared to fully directional spectra from the NOAA and non-directional spectra from the NDBC. In order to continue this aspect of the study, fully directional spectra from FNMOC is required. Using the full spectra the parameters value necessary to use higher order spectral shape functions may be identified, improving the accuracy of the synthesized spectra.

Figure 3.12 shows the relative importance of each of the environment, model or solution parameters investigated in this chapter. Based on these findings it is recommended that the SWAN model of this chapter use an unstructured grid, operate in non-stationary mode, include wind forcing at the highest spatial resolution available and use wave boundary conditions at the highest available spatial and spectral resolution.

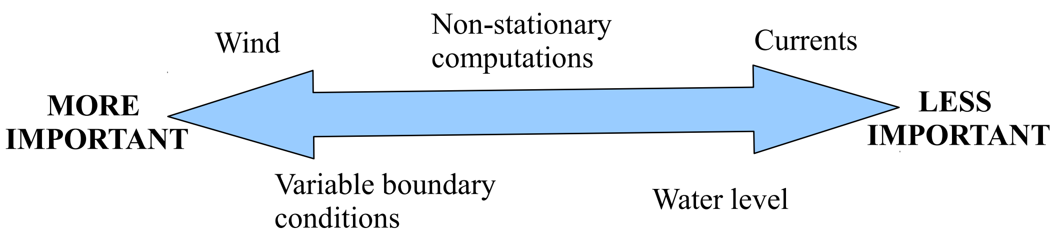

Figure 3.12: Relative importance of various environmental, modelling and solution parameters.

Chapter 4

Wave Modelling with REF/DIF - A Case Study

This chapter presents a case study of the wave climate in Hesquiaht Sound, a small sub region of the medium scale domain investigated in chapter 3. The near-shore wave climate was determined by using REF/DIF to evaluate the most frequently occurring sea-state in each month rather than by hind-casting or forecasting. In this way a snap-shot of the typical near-shore wave climate in each month was attained without the expense of copious model runs. Because wind cannot be accounted when selecting the most frequently occurring seas, and because REF/DIF cannot simulate wave generation by wind, wind was not accounted for and is therefore a limitation of this study. REF/DIF was used for this study because of the presence of a large blocking peninsula and several small head-lands around which diffraction is likely important. The use of REF/DIF amounts to a trade-off of improved simulation of diffraction for the inability to simulate wave growth by wind.

This study uses boundary conditions sourced directly from the NOAA's WW3 model. The quality of the boundary conditions may have been improved if a medium scale model such as the one discussed in the previous chapter was used, but the work in the current chapter was performed before that of chapter 3. Since the depth at the outer boundary of the model is approximately 150m, it is still expected that the WW3 results will have adequate accuracy.

The work which forms the basis of this chapter was commissioned to the author by SyncWave Energy Inc. The objective was to evaluate the suitability of the wave climate of Hesquiaht Sound for deployment of wave energy conversion devices.

Hesquiaht Sound is the northern portion of Clayquot Sound on the West Coast of Vancouver Island. Within Hesquiaht Sound is Hot Springs Cove, the permanent residence of the Hesquiaht First Nation (see Fig. 4.1). This community of approximately 200 residents is completely reliant on imported diesel fuel for electricity generation. The high cost, cost uncertainty and environmental damage associated with diesel based electricity generation have prompted interest in renewable alternatives, including wave energy. The case study that follows uses eight years of wave data to characterize the wave climate of Hesquiaht Sound on a monthly basis. Special attention is given to issues important to siting a WEC to service Hot Springs Cove.

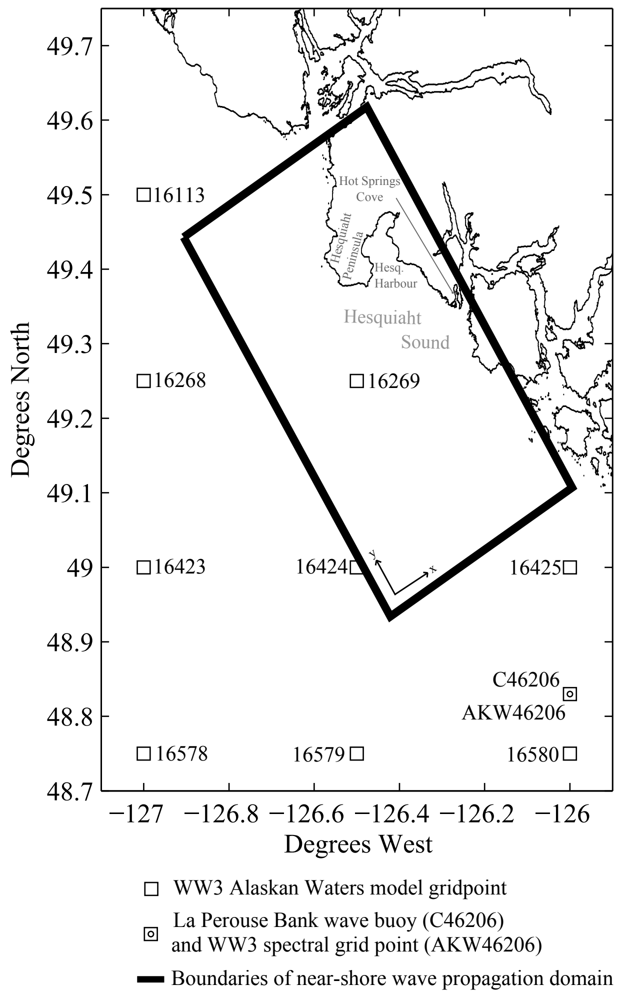

Figure 4.1: Map showing Hesquiaht Sound, WW3 Alaskan Waters Model grid points, buoy location and domain of wave propagation model

4.1 Resource Assessment Methodology

Like [10], the wave resource assessment methodology used here is multi-stage. A flow chart of the method is shown in Fig. 4.2. First, multiple years of off-shore wave climate data are collected. Note that in this chapter *off-shore* refers to the sea-ward boundary of the computational domain shown in Fig. 4.1. It is different from the off-shore boundary refereed to in chapter 3. Because the target region is small, data from only a few locations on the off-shore boundary are required. Archives of parametric wind-wave model results are used as the primary data source and are locally validated by comparison to *in-situ* measurements (see upper portion of Fig. 4.2).

Following validation of the parametric archives, characteristic sea-states are defined corresponding to the peak value of each month's H_s, T_p, θ_p joint probability distribution (JPD). The average wave conditions are not used because waves from large storms can significantly skew those averages and WECs will be unable to operate in these high seas and will default to a *survivability mode* in which little energy is converted. The peak value of the joint probability distribution is influenced very little by these storm events and is a better indicator of typical operating conditions.

Spectra best matching the characteristic sea-states are selected from an archive of off-shore spectral WW3 data (see middle of Fig. 4.2). To estimate the near-shore sea-states, the characteristic off-shore wave spectra are used as boundary conditions to the near-shore wave propagation model, REF/DIF-1. This is unlike most WRA executions, where wave spectra are synthesised from H_s, T_p and θ_p.

Propagation of each spectrum is simulated by a separate execution of REF/DIF for each monochromatic wave component. Then the wave theory of Section 1.1.1 is used to aggregate the results. For each month this yields characteristic wave spectra over the entire near-shore domain (see bottom of Fig. 4.2).

4.2 Data Sources

Two types of data are necessary to complete this study: bathymetric and off-shore wave climate.

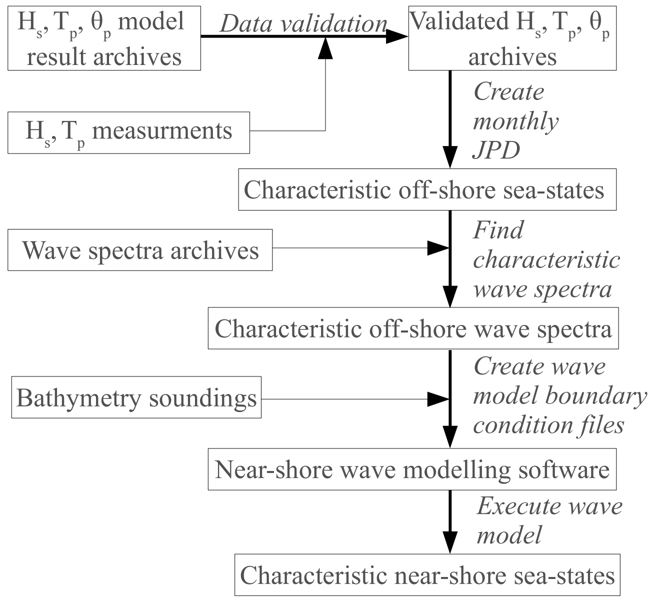

Figure 4.2: Flow chart showing the steps in the proposed wave resource assessment methodology.

4.2.1 Bathymetry

The grid resolution needed to capture the fine-scale geographic variability of wave climate very close to shore is much greater than even the smallest grid dimension of the *WXCIx2* grid used in the previous chapter. In REF/DIF, bathymetric soundings at each point in the computational grid are a required boundary condition. Bathymetric data for this study was obtained from the Canadian Hydrographic Service (CHS). The bathymetric grid used in this chapter and shown as contours in Fig. 4.3 was produced by first extracting *x,y,z* positional scatter from bathymetric shape-files supplied by the CHS. In total there were 480,000 soundings at varying density. Next, the geographic references were then converted to the meters based *Universal Transverse Mercator* referencing system. The data was then interpolated onto a regular, rotated grid at 50m spacing using Matlab's *griddata* function. Where necessary, REF/DIF performed additional interpolation of the 50m grid in order to maintain five grid points per wavelength.

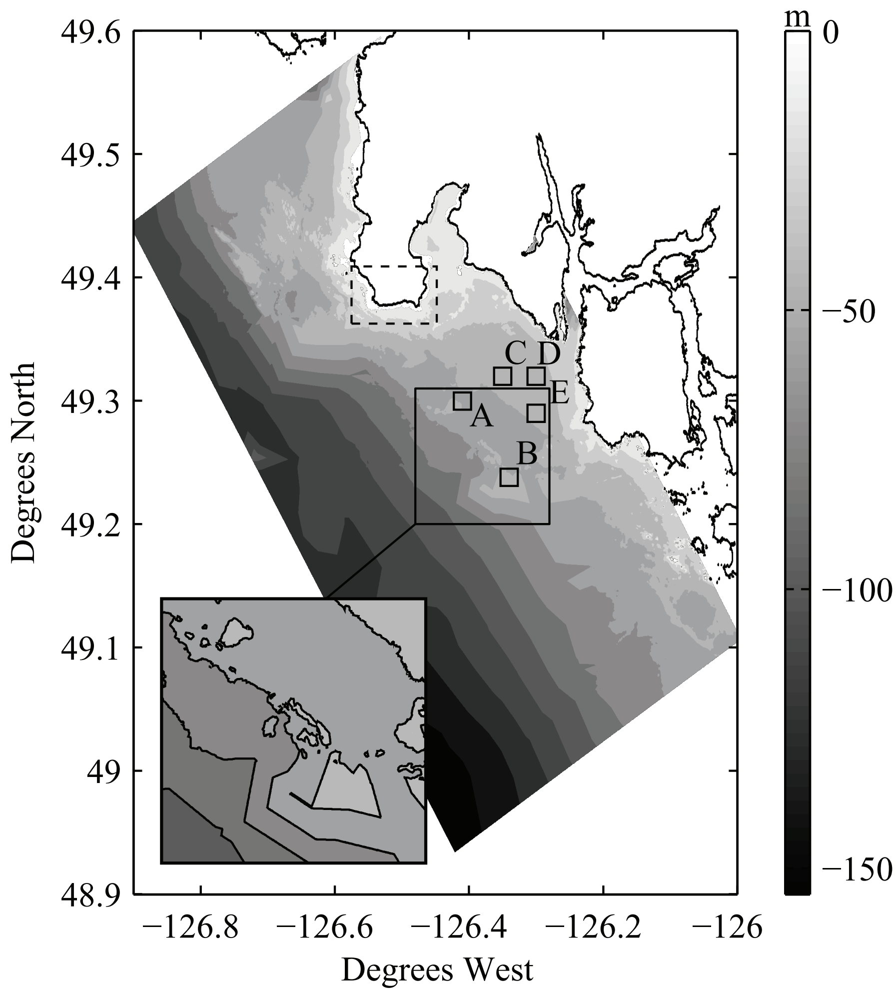

Figure 4.3: Bathymetric contours in the near-shore propagation model domain and selected near-shore sites A-E. Dashed rectangle indicates location of Fig. 4.4.

Near-shore sites A-E indicated in Fig. 4.3 are discussed in detail in Section 4.5. The computational grid around the tip of Hesquiaht Peninsula and associated headlands are shown in Fig.4.4.

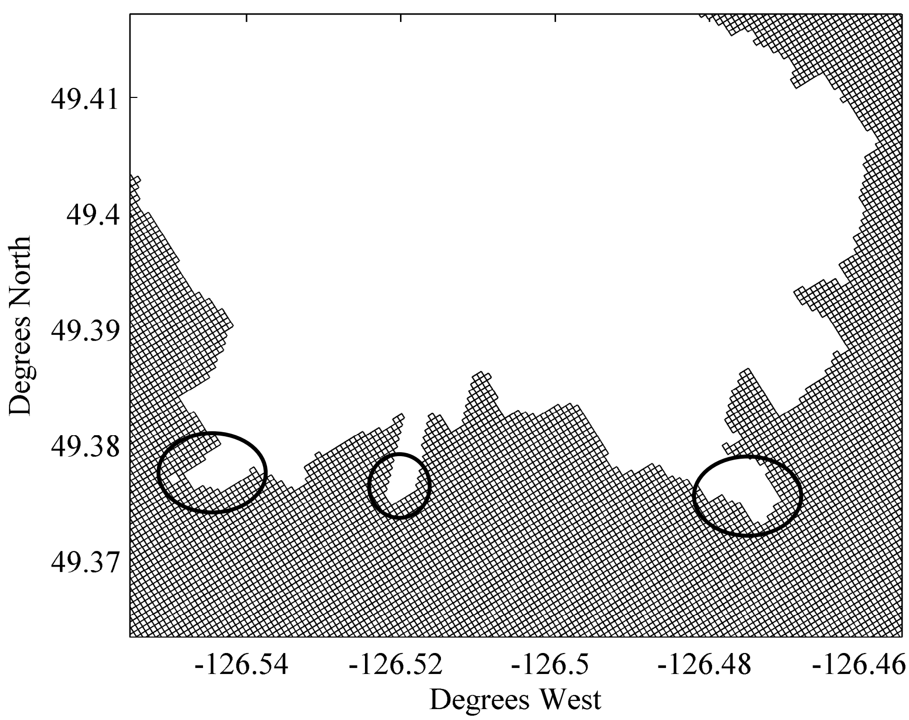

Figure 4.4: The computational grid around Hesquiaht Peninsula (see dashed rectangle in 4.3). Headlands and points where diffraction is thought to be important are indicated with black oval.

4.2.2 Off-shore Wave Data

Three data-sets of archived statistical wave parameters (H_s, T_p and θ_p) were acquired for this study. Two gridded WW3 data-sets were acquired from the NOAA, one from the Alaskan Waters Model (AKW) covering July 1999 to November 2007 and the other from the Eastern North-Pacific Model (ENP) covering August 2002 to November 2007. One measured data-set was acquired from the Canadian Department of Fisheries and Oceans (DFO) for buoy C46206 (see Figs. 3.1 and 4.1) at La Perouse Bank covering November 1988 to November 2008. This dataset was used to select a valid WW3 data set. Though the wave buoy data set is much larger than the the WW3 data sets, it has several shortcomings: its location is significantly south-west of Hesquiaht Sound; the data set is discontinuous; and, more seriously, the buoy does not measure wave directionality and is therefore not appropriate as a boundary condition for near-shore wave propagation modelling.

4.2.3 Wave Data Verification

To assess the local performance of the WW3 models and to choose which data set is best suited to this study, each WW3 data-set was compared at the closest available grid point to the data set from buoy C46206. As in [3] model performance is assessed based on bias, scatter index and correlation coefficient (Eqns. 2.4-2.7). Table 4.1 gives the location, depth and sampling period (T_s) of the data stations used in model validation.

Before comparing the buoy and WW3 data, quality assurance was performed on the buoy data. All buoy measurements are assigned an Integrated Global Ocean Services System quality code by the DFO (including *no QA performed*. All measurements with a quality code of *Erroneous* or *Doubtful*, or a H_s value of zero, were eliminated. Measurements with the *no QA performed* code (a large portion of the

Table 4.1: Data stations for WW3 model validation

Name-point	Location	Term	Depth (m)	T_s (hr)
AKW16580	48.75N 126.0W	1999/07- 2007/11	91	3
ENP17709	48.75N 126.0W	2002/08- 2002/08	91	3
C46206	48.83N 126.0W	1988/11- 2008/11	72	1

data-set) were retained. The buoy measurement closest in time to the model result was used for comparison with a difference limit of three hours.

As in Section 2.2, Table 4.2 gives the local WW3 validation statistics for both the AKW and the ENP Models. For both models correlation is higher and bias is lower for H_s than for T_p. For both models the H_s bias is positive, which is consistent with WW3's tendency to over predict wave height [53], but may also result from the WW3 grid point being located farther from shore and in deeper water than buoy C46206. Though the performance of the models are nearly equal, the AKW Model shows slightly lower bias of H_s and T_p. Given the mildly superior performance and longer duration of the AKW Model, it was selected as the primary data source for this study.

Table 4.2: Table of WW3 local validation statistics (see Eqns. (2.3-2.7)).

	Model	Pairs	mean	B	SI	r
H_s (m)	AKW	18760	2.10	0.29	0.26	0.89
	ENP	11077	2.20	0.31	0.30	0.88
T_p (s)	AKW	18760	10.82	-0.53	0.23	0.61
	ENP	11077	10.97	-0.60	0.22	0.61

The boundaries of the near-shore computational grid are given in Fig. 4.1. The boundary extends from roughly 49.5°N,127°W to 49°N,126.5°W. The two WW3-AKW grid points defining this boundary were examined for continuity. The two points were compared using Eqns. (2.3-2.7), with the point at 49°N,126.5°W used as the reference. The results given in Table 4.3 show that these points exhibit excellent continuity and do not require that a variable boundary condition be used. The negative bias in direction is likely due to the fact that the one grid point is farther shore-ward from the continental shelf and the waves experience some turning due to refraction as the waves pass over the shelf. Wave data from the most appropriately located grid point, #16426, of the AKW Model was selected as the primary data source for this study.

Table 4.3: Validation statistics for WW3-AKW grid points 16113 and 16424 on the off-shore boundary of the wave propagation model domain

Locations		mean	B	SI	r
49.5°N,127°W 49°N,126.5°W	H_s (m)	2.48	-0.16	0.09	0.99
	T_p (s)	10.29	0.05	0.17	0.81
	θ_p (°)	258.7	-6.14	0.07	0.84

4.2.4 Off-shore wave climate characterization

All eight years of archived H_s, T_p and θ_p data from AKW16426 were used to produce the monthly joint probability distributions. Direction, period and wave height integrated projections of each distribution is shown in Fig. 4.5. The the wave parameters corresponding to the maximum value of the joint probability distribution represent the most frequently occurring sea-state. Table 4.4 gives the wave parameters corresponding to the mean and maximum value of each distribution (maximum values denoted by *).

The seasonal progressions of H_s, T_p and θ_p are readily apparent in columns a, b and c of Fig. 4.5. Also visible in Fig. 4.5 is a secondary local maximum in the probability distribution during May through August. This secondary local maximum consists of long period swell from south, south-west. This swell, generated by winter storms in the Southern Ocean, traverses the Pacific Ocean to arrive in Hesquiaht Sound. As a result of this secondary swell, the wave spectra of the summer are typically double

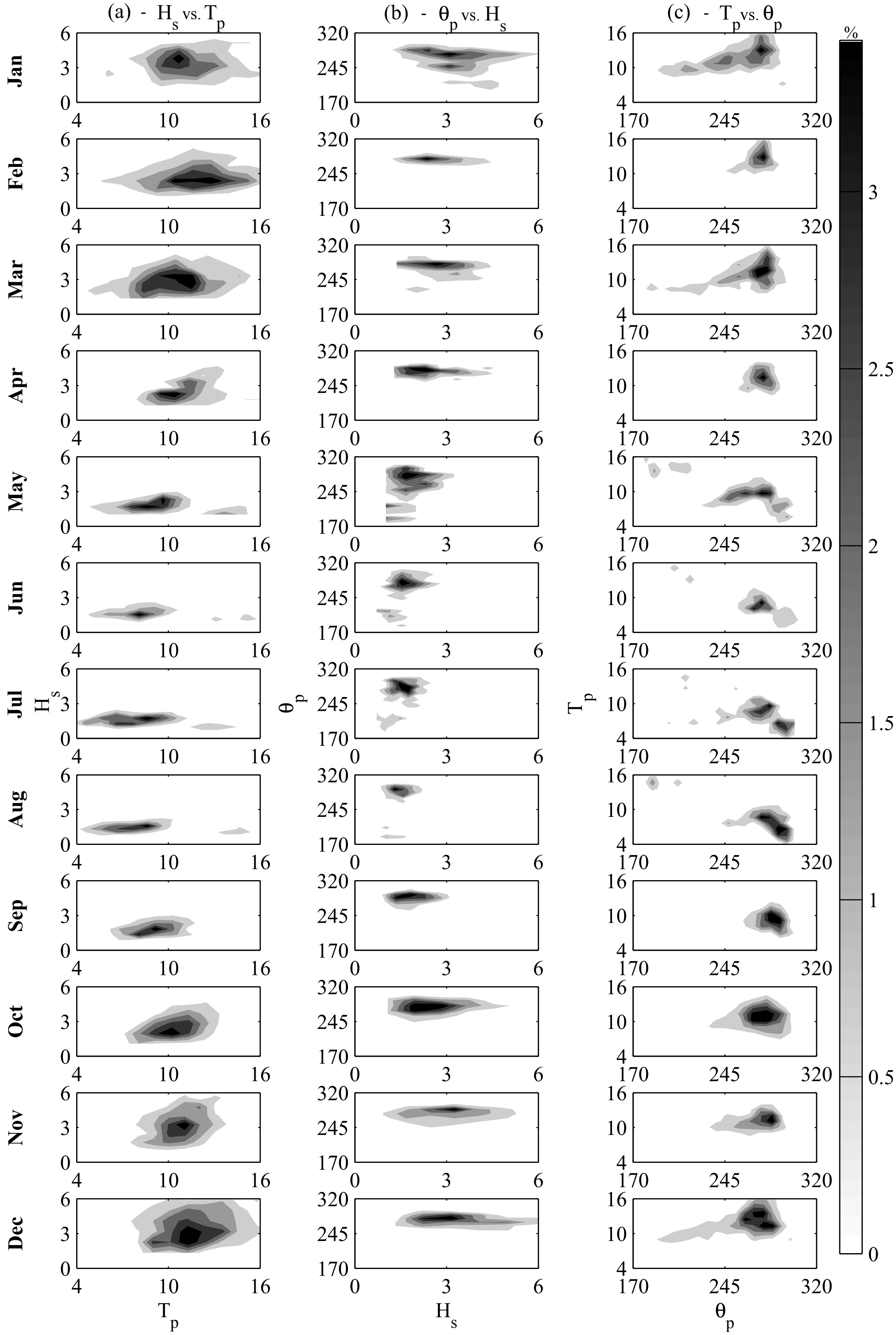

Figure 4.5: The (a) θ_p integrated, (b) T_p integrated, (c) H_s integrated projection of joint probability distribution by month for AKW16424. Number of bins in each dimension is 10, 15, 24 for H_s, T_p, θ_p respectively.

Table 4.4: Mean and characteristics sea-state parameters at AKW-16424.

Month	$\overline{H_s}$(m)	H_s^*(m)	$\overline{T_p}$(s)	T_p^*(s)	$\overline{\theta_p}$(°)	θ_p^*(°)
Jan	3.4	2.8	11.4	11.3	248	244
Feb	2.8	2.0	11.8	12.2	258	273
Mar	3.0	2.4	10.6	11.0	251	276
Apr	2.6	2.0	10.9	10.9	261	274
May	1.8	2.0	10.0	9.1	251	279
Jun	1.7	1.3	9.2	7.6	259	278
Jul	1.6	1.6	8.4	8.1	259	271
Aug	1.4	1.4	8.9	8.1	263	272
Sep	1.9	1.6	9.6	8.6	270	286
Oct	2.7	1.5	10.5	9.7	265	262
Nov	3.3	2.9	10.9	10.6	259	279
Dec	3.7	2.7	11.7	13.0	254	273

peaked as shown in Fig. 4.6a and consequently are not well modelled by synthetic single peaked spectra such as JONSWAP or Pierson-Moskowitz.

To find accurate off-shore wave spectra for the Hesquiaht region, an additional data set containing full directional spectra, was obtained by periodic download of NOAA AKW Model forecasts from April to November, 2009. The NOAA provides directional spectra only for selected grid points and, until recently, the spectra were not archived. The closest available WW3 spectral grid point is at 48.83°N,126°W, the same position as the buoy C46206 (see Fig. 4.1). Though approximately 30km SW of the outer boundary of the computational domain, this is the closest directional spectral data available and is close enough that it can be expected to exhibit the same climate trends.

Spectral wave boundary conditions for the propagation model were selected by searching for the best-fit match to the characteristic monthly sea-state within archived WW3-AKW wave spectra. For the months having directional wave spectra available, the *most characteristic* spectra within a month j was determined as that which minimizes X.

$$X_j = \frac{|\vec{H}_{sj} - H_{sj}^*|}{H_{sj}^*} + \frac{|\vec{T}_{pj} - T_{pj}^*|}{T_{pj}^*} + \frac{|\vec{\theta}_{pj} - \theta_{pj}^*|}{\theta_{pj}^*}. \tag{4.1}$$

Here $\vec{H}_{sj}$, $\vec{T}_{pj}$ and $\vec{\theta}_{pj}$ represent the archives of directional spectra for month j. For the months where no spectral wave data was available (December-March), spectra were synthesized using the Pierson-Moskowitz spectrum with cosine squared directional spreading [2].

4.3 Near-shore wave modelling using REF/DIF-1

Propagation of a wave spectrum was simulated by modelling each discrete component of the spectrum separately and then applying the wave theory of Section 1.1.1 to aggregate the results. REF/DIF's monochromatic breaking scheme is used to dissipate wave energy at shore, but since a spectrum of wave components was propagated, the breaking scheme is not valid. A spectral breaking scheme such as the one employed in REF/DIF-S would need to be implemented in order to expect accurate results within the surf zone.

Further invalidating the monochromatic breaking scheme was the change of the wave breaking energy dissipation coefficient, κ, from 0.15 to 0.017. This change was made to minimize the introduction of high wave-number noise caused by wave breaking around islands and headlands (as discussed on p.19 of [46]).

As shown in Fig. 4.1, the domain of the wave propagation model was oriented such that the boundaries are roughly parallel and perpendicular to the shore-line. Orienting the domain in this way allows more of the predominant sea-states to be captured within the +/-70° aperture of REF/DIF than a north-south oriented grid would allow. Additionally, the algorithm used by REF/DIF to allow waves to travel obliquely in and out of the domain is most effective when those boundaries are oriented in a shore-ward direction. The domain is much wider than it is long to ensure that waves propagating at oblique angles reach the area of interest in Hesquiaht Sound.

4.4 Wave Spectra clipping

To use the selected WW3 wave spectra as boundary conditions to REF/DIF, some *clipping*, or removal of extraneous wave components, was necessary. Spectra were clipped to remove wave components outside +/-65° (relative to model domain x-axis shown in Fig. 4.1) in order to adhere to REF/DIF's +/-70° wave angle limitation. Wave components of period less than 5 seconds were also clipped. Modelling low energy, high frequency, short wavelength waves is problematic as REF/DIF requires at least 5 grid points per wavelength and will interpolate the computational grid if necessary in order to satisfy this condition. The power in the off-shore and propagated spectra, as well as the percentage of power clipped from each characteristic spectrum is given in Table 4.5.

Table 4.5: Spectrum power loss due to clipping of spectra

Month	Off-shore J (kW/m)	Propagated J (kW/m)	Clipped J (%)
Jan	40.9	39.5	3.48
Feb	23.9	20.0	16.4
Mar	29.1	23.5	19.0
Apr	18.0	15.3	15.2
May	16.1	15.2	5.5
Jun	7.0	5.9	16.1
Jul	9.1	7.1	22.1
Aug	8.6	7.8	8.6
Sep	11.6	10.2	11.9
Oct	9.1	7.8	14.1
Nov	31.79	28.8	9.5
Dec	45.9	38.5	16.1

During some months, as much as 22% of spectrum power was clipped. This appears significant, but most of the clipped power is coming from the north-east and is shielded from a large portion of the Sound by the Hesquiaht Peninsula. This point is illustrated by Fig. 4.6 which shows the un-clipped and clipped characteristic spectrum for September. The projections of the spectrum on the x-z and y-z planes show that only high frequency components and components coming from north of 300° are clipped.

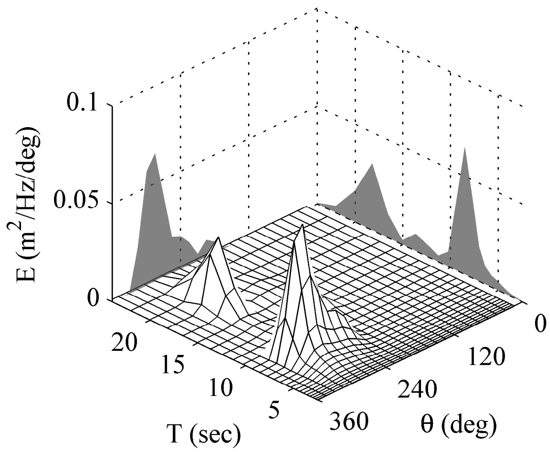

(a)

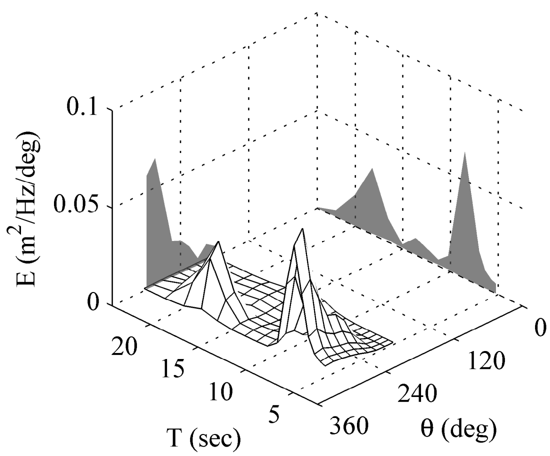

(b)

Figure 4.6: a) Unmodified characteristic spectrum for September and, b) clipped characteristic spectrum for September.

4.5 Results and Discussion

The characteristic wave spectra were propagated though the computational domain using REF/DIF-1. Complete wave spectra were computed and saved at every location in the computational domain. From the recorded spectra, parameters J, H_s, T_p, T_e

and θ_p were computed. Figure 4.7 shows the wave power and primary direction over the area of interest near Hot Springs Cove for January, April, July and October.

Indicated in Fig. 4.7 are selected near-shore points A-E. These points were selected strictly for illustrative purposes at depths generally appropriate to both slack and tight moored WECs [54].

Visible in all plots in Fig. 4.7 are two major sets of power striations. Points A and B sit roughly at their origin and C, D and E in the developed regions. The striations are caused by sea-mounts, both visible in Fig. 4.3 (see inset). As waves pass over the sea-mounts they refract, or bend so that the wave-fronts are turned toward themselves causing an energy focusing effect. Though the effect is a real result of refraction and diffraction, the power in the waves behind the sea-mounts would likely be more spatially smoothed than predicted. The direction bins used by WW3 and implemented in this near-shore model are 15° wide. In a real sea, the energy within that bin would be roughly equally distributed throughout the 15°, here the energy has been concentrated in a single direction, numerically accentuating the focusing effect.

The monthly characteristic wave power transport at locations A-E are given in Fig. 4.8. All exhibit monthly power transport variation similar to that of the off-shore. As expected, the further off-shore sites A and B typically retain more power than the sites nearer to shore. More of the off-shore power is retained during the summer months because the typically high-frequency, short wavelength waves interact with the ocean floor over a shorter distance than the low frequency waves of the winter, and thus lose less energy. Figure 4.9 gives monthly variation of H_s, T_p, T_e and θ_p, both off-shore, and for near-shore sites A-E. Near-shore, H_s follows the off-shore trend but is reduced due to bottom friction and spectrum clipping. T_e follows the off-shore trend, except in the summer when short period waves removed by the spectrum clipping operation cause an increase in T_e. The unstable parameters T_p and θ_p are generally close to the off-shore value but, in some instances, jump to a high energy component in a different region of the wave spectrum.

The evolution of the sea-state as it approaches shore can be quantified by the *wave power transport coefficient*, η, which is the ratio of near-shore to off-shore power transport, J. Shown in Fig. 4.10 is the monthly variation of η. For all near-shore sites, η exhibits a seasonal variability, with larger values during the summer and smaller values in the winter. This results from both the change of wave focal points behind the near-shore sea-mounts due to shifting wave direction and the tendency of longer period waves of the winter to lose more energy to bottom friction. July does not follow this seasonal trend because significant high frequency energy is removed from spectrum during the clipping process and because a large portion of the energy in the wave spectrum is travelling oblique to the x-direction, increasing the distance waves must travel to reach the near-shore sites and thus increasing energy loss. January does not follow the trend because θ_p is directed precisely towards Hot Springs Cove, which minimizes propagation distance to the near-shore sites and thus reduces energy loss. The average η for points A, B, C, D and E is 0.80, 0.79, 0.60, 0.66 and 0.59 respectively.

Site D, the closest to Hot Springs Cove (4km to landfall and 5.75km to the town), has on average 66% of the off-shore resource, or 13.1kW/m of wave power transport. This shows that even very close to Hot Springs Cove the wave resource is still very powerful and likely appropriate for deployment of wave energy conversion technologies.

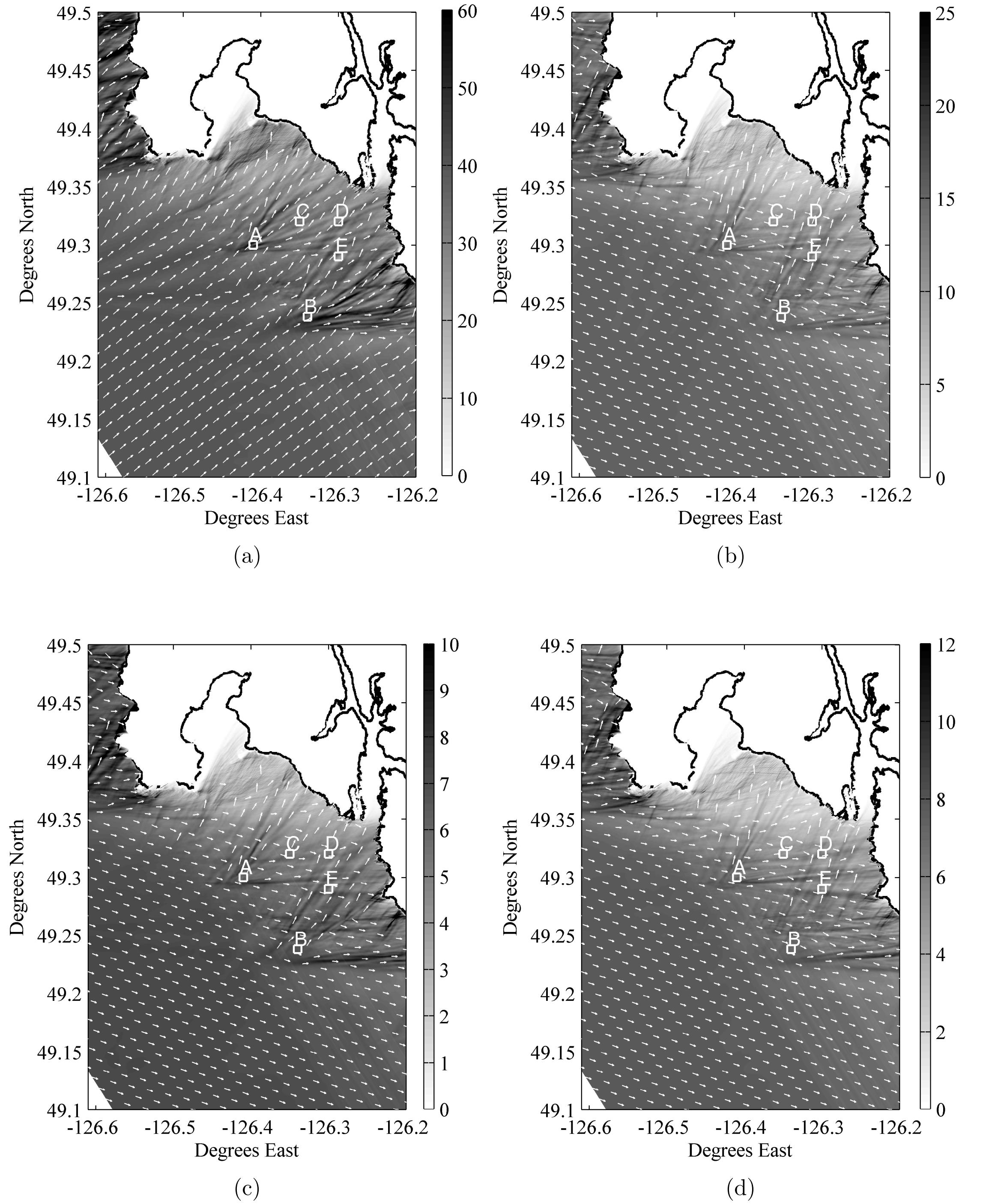

Figure 4.7: Wave propagation results for January, April, July and October characteristic sea-states. Surface contours represent wave power transport in kW/m, quivers indicate peak wave direction

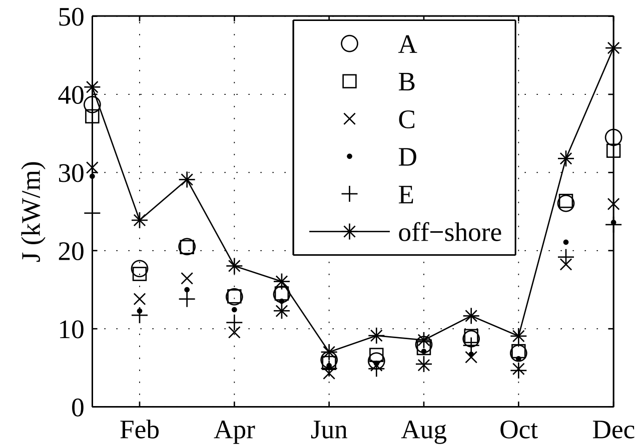

Figure 4.8: Wave power transport of near-shore locations A-E and off-shore.

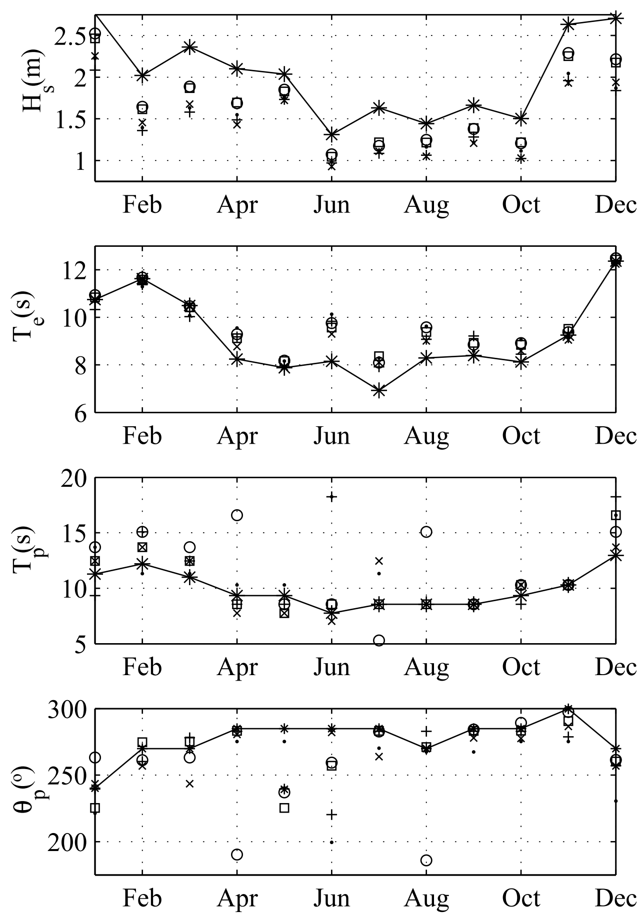

Figure 4.9: H_s, T_p and θ_p off-shore and for selected near-shore points A-E

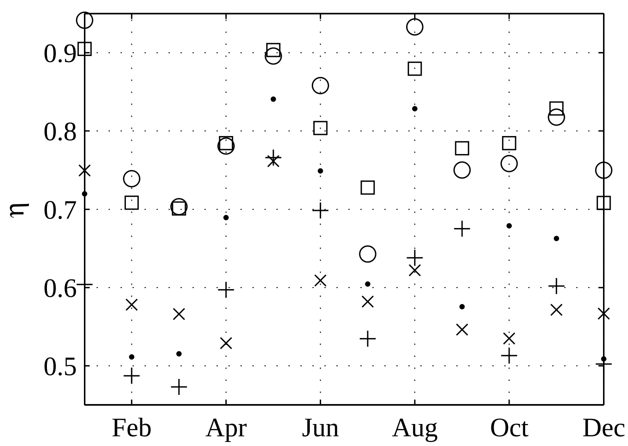

Figure 4.10: Wave power transport coefficients for selected near-shore sites A-E.

4.6 Further Comments

4.6.1 Directional binning

The frequency and direction binning used in this case study were based on the binning of the WW3 input data. The direction bin width was 15° and the frequency bin width varied from 0.004-0.018Hz. The direction and frequency discretization necessary to adequately simulate waves on a open coastline over the narrow continental shelf of the Pacific was explored in [45]. The authors found that a direction bin width of 5° and frequency bandwidth of 0.01Hz was sufficient to produce accurate results. Unfortunately, larger bin widths were not tested. The expected accuracy using a 15° directional bin-width has not been investigated and requires further study.

4.6.2 Winds, tides and currents

As characteristic sea-states representative of entire months were used in this case study, winds, tides and currents were neglected. If a near-shore climate forecasting/hind-casting system were to be set-up, the influence of winds, tides and currents on wave estimates would need to be considered as was done in chapter 3. If the influence of wind was found to be significant, then the trade-off between better simulation of diffraction and the inability to simulate wave growth by wind, inherent in selecting REF/DIF over SWAN, may have to be reconsidered. To obtain current and water level estimates, a separate marine circulation modelling package is generally required.

4.6.3 Model validation and calibration

In response to the limitations inherent in wave propagation modelling, it is suggested that commercially driven modelling efforts use *in-situ* measurements for verification and calibration of the near-shore model. This requires at least one measurement device, but greatly increases the value of the modelled data. Using a single wave buoy to verify near-shore model results is still expected to be vastly less expensive than characterizing a near-shore wave climate with measurements from multiple buoy deployments.

As previously discussed, one such program is currently under way on the West Coast of Vancouver Island. The West Coast Wave Collaboration Project, headed by the University of Victoria has deployed a wave buoy at Amphitrite bank near Ucluelet, BC. The buoy will be used to establish the potential of the area for deployment of wave energy conversion technologies and to validate a SWAN forecast/hind-cast model of the region.

4.7 Summary

This chapter describes a case study of the wave climate of Hesquiaht Sound, BC, Canada. It was found that in the area of interest, near the Village of Hot Springs Cove, the wave power transport is typically 60% to 80% of the off-shore value. One of the selected near-shore sites (D), the closest to Hot Springs Cove (just 4km to landfall and 5.75km to the town), shows particular promise. This location has on average 66% of the off-shore resource, or 13.1kW/m of wave power transport. Site 'D' shows that even very close to shore, the wave resource is still powerful and likely appropriate for deployment of wave energy conversion technologies.

Chapter 5

Conclusions

The forthcoming wave energy industry has the potential to make a real contribution to our future carbon-reduced energy economy. To realize this potential those developing wave energy devices require efficient and economic access to near-shore wave data. For the West Coast of Vancouver Island no such data-set exits. To aid in correcting this deficiency this thesis provides a framework for estimating near-shore conditions, specifically on the West Coast of Vancouver Island through the use of computational wave models.

Chapter 1 discussed select off-shore and near-shore wave models, their derivation and appropriate application. Off-shore models such as WAM, WW3 and the BMOWM are governed by the spectral action density equation, which is derived from the principle of energy conservation. These models provide good wave estimates off-shore but fail near-shore because they do not include handling for some of the physics which become important in shallow water. However, the results from off-shore models are a valuable source of boundary conditions for near-shore models and are used extensively throughout this thesis.

Chapter 2 discussed two near-shore models, SWAN and REF/DIF. SWAN is based on the same governing equation as the off-shore models, but additionally includes handling of most near-shore physics. SWAN has difficulties simulating diffraction, which can become important very close to shore, but is formulated such that it is applicable over a wide range of spatial scales. REF/DIF is based on the mild-slope equation and solves for the free surface condition. It contains a more exact handling of diffraction, but also requires at least five grid points per wave-length. The computational expense associated with this requirement limits the use of REF/DIF to areas less than a few hundred kilometres. SWAN and REF/DIF may be used in a complementary fashion, where SWAN is used at an intermediary between the global-scale off-shore models and the detailed, small scale computations of REF/DIF. When operating SWAN at this medium scale a number of other environmental factors become important.

Chapter 3 examined the sensitivity of wave estimates from a medium scale SWAN model of the West Coast of Vancouver Island. Computations were made on an unstructured grid which allowed the grid resolution to vary throughout the domain. A study of the sensitivity of wave estimate to grid resolution showed that a grid resolution close to that of the source bathymetry was the most appropriate. A study of wind effects showed both wind speed and spatial resolution of the wind field have significant effect on wave estimates. The effect of tidal heights and currents were investigated; except near the surf zone, little sensitivity was found. A comparison of stationary and non-stationary computations showed that non-stationary computations do not necessarily differ in accuracy from stationary computations and are much more computationally efficient. The influence of the resolution of the wave boundary conditions on wave estimates was studied. The results show that wave estimates are sensitive to both the spatial and spectral resolution of the wave boundary conditions. Based on these findings it is recommended that a medium-scale SWAN model such as the one used in chapter 3 use an unstructured grid, operate in non-stationary mode, include wind forcing at the highest spatial resolution available and use wave boundary conditions at the highest available spatial and spectral resolution.

Chapter 4 presented a case study of the wave climate in Hesquiaht Sound, a small sub region of the medium scale domain investigated in chapter 3. REF/DIF was used for this study because presence of a Hesquiaht Peninsula which has several headlands around which diffraction was thought to be important. The near-shore climate was characterized by modelling the most frequently occurring sea of each month. The results showed large variation in the wave energy between the off-shore boundary and shore. Throughout the year the off-shore wave power varies between 7 and 46kW/m. A selection of near-shore sites typically have 69% of the offshore power and range from 5 to 39 kW/m throughout the year. One near-shore site located close to Hot-Springs Cove, has on average 13.1kW/m of power, a significant amount likely sufficient for wave energy development.

The framework for near-shore wave climate assessment presented in this thesis may be used by groups or individuals to assess the wave climate in near-shore regions of the West Coast of Vancouver Island or other regions of the world where wave energy extraction may be promising. It is only with detailed knowledge of the wave climate that we expect commercial extraction of wave energy to commence.

5.1 Contributions

This thesis has made several contributions to the academic and industrial wave energy community. It has:

1. demonstrated the utility of near-shore wave modelling software for procuring near-shore wave data for those developing wave energy devices.

2. shown the value of off-shore wave data calculated by global wind-wave models such as WAM and WW3 as boundary conditions for near-shore models.

3. identified the environmental factors (wind, currents, tidal elevation), modelling options (grid geometry, grid size, solution type) and wave boundary condition resolution (spectral, spatial, temporal) necessary for an accurate and efficient SWAN model of the West Coast of Vancouver Island.

4. demonstrated wave resource assessment in a case study of Hesquiaht Sound.

5. and shown that, for the most frequently occuring wave spectra, the wave power near-shore in Hesquiaht Sound to range 5 to 39kW/m.

5.2 Recommendations

For those attempting to perform wave resource assessment in support of wave energy development, this research has yielded several recommendations:

1. Use the appropriate wave model. Different wave models are appropriate for different applications. Identify you primary requirements and select a wave model which will best satisfies those requirements.

2. Model only what you need. If an understanding of the spatial variability of the wave field near-shore is required, then modelling of the most frequently occurring seas may be most appropriate as was performed in chapter 4. If it is necessary to know the near-shore wave field at discrete points in time a hindcast or forecasting model may be required such as the one in development in chapter 3.

3. Model only the important physics. Keeping the model simple will reduce development time and ease trouble-shooting. Identifying the important physics may, however, require sensitivity studies similar to those performed in chapter 3.

4. Use the best available wave boundary conditions. This may require validation against other trusted data sources

5. Where possible, validate the results of the near-shore model with *in-situ* measurements. This is the only definitive method for evaluating the accuracy of the model.

5.3 Further Work

There are many areas where the work presented in this thesis could be furthered. The most important of these are as follows:

1. The influence of using high fidelity, high spatial resolution boundary conditions on SWAN wave model prediction was not assessed due to lack of appropriate data. The influence of these boundary conditions may have to be assessed in a region where appropriate data is available. Alternatively, the data could be produced by purpose runs of a global wave model such as WW3.

2. The accurate synthesis of directional wave spectra from parametric data was only briefly addressed in this thesis. It would be valuable to investigate how higher order spectral shape functions may be effectively utilized. This may involve using available directional spectra to identify the appropriate values of the additional parameters necessary to define these higher order functions.

3. The recommendations of chapter 3 were not executed. With those recommendations a hind-casting/forecasting model of the West Coast of Vancouver Island could be set-up. This would be of great value to the wave energy community. The model could even be calibrate and validated to the directional wave buoy currently deployed by the West Coast Wave Collaboration Project.

4. The wave calculations made in Chapter 4 were not validated. Significant additional value could be realized if the results of those wave calculations could be validated by comparison to *in-situ* measurements.

Bibliography

[1] L.H. Holthuijsen. *Waves in Oceanic and Coastal Waters*. Cambridge University Press, 2007.

[2] K. M. Ochi. *Ocean Waves: The Stochastic Approach*. Cambridge University Press, 1998.

[3] Jean-Raymond Bidlot, Jian-Guo Li, Paul Wittmann, Manon Fauchon, Hsuan Chen, Jean-Michel Lefevre, Thomas Bruns, Diana Greenslade, Fabrice Ardhuin, Nadao Kohno, Sanwook Park, and Marta Gomez. Inter-comparison of operational wave forecasting systems. In *10TH INTERNATIONAL WORKSHOP ON WAVE HINDCASTING AND FORECASTING AND COASTAL HAZARD SYMPOSIUM*, 2007.

[4] Mollison, Buneman, and Salter. Wave power availability in the NE Atlantic. *Nature*, 263:223–226, 1976.

[5] S.H. Salter. Wave power. *Nature*, 249(5459):720–4, June 1974.

[6] J.A. Crabb. Assessment of wave power available at key United Kingdon sites: a description of work in Department of Energy's Wave Energy Programme. Report 186, Institute of Oceanographic Sciences, 1984.

[7] Denis Mollison. Wave climate and the wave power resource. In *Hydrodynamics of Ocean Wave-Energy Utilization*, pages 133–156. Springer, 1986.

[8] Denis Mollison. The UK wave power resource. *Wave Energy, I Mech Eng*, pages 1–6, 1991.

[9] T J T. Whittaker and D. Mollison. The UK shoreline and nearshore wave energy resources. Technical Report ESTU WV 1683, UK Department of Trade and Industry., 1992.

[10] M.T. Pontes, D. Mollison, L. Cavaleri, G.A. Athanassoulis, and J.C. Nieto. Wave studies and development of resource evaluation methodology. Final Report, Contract DGXII N° JOUR-132-PT(MNRE), 1993.

[11] C. Beels, J.C.C. Henriques, J. De Rouck, M.T. Pontes, G. De Backer, and H. Verhaeghe. Wave energy resource in the North Sea. In *Proceedings of the 7th European Wave and Tidal Energy Conference*, 2007.

[12] A. Beyene and J.H. Wilson. Digital mapping of California wave energy resource. *International Journal of Energy Research*, 31(12):1156–1168, 2007.

[13] Andrew Cornett and J. Zhang. Nearshore wave energy resources, Western Vancouver Island, B.C. Technical Report CHC-TR-51, Canadian Hydraulics Centre, April 2008.

[14] M. Folley and T.J.T. Whittaker. Analysis of the nearshore wave energy resource. *Renewable Energy*, 34(7):1709–1715, July 2009.

[15] G. Iglesias and R. Carballo. Wave energy and nearshore hot spots: The case of the SE Bay of Biscay. *Renewable Energy*, 35(11):2490–2500, November 2010.

[16] G. Iglesias and R. Carballo. Wave energy resource in the Estaca de Bares area (Spain). *Renewable Energy*, 35(7):1574–1584, 2010.

[17] G. Iglesias, M. Lpez, R. Carballo, A. Castro, J.A. Fraguela, and P. Frigaard. Wave energy potential in Galicia (NW Spain). *Renewable Energy*, 34(11):2323–2333, November 2009.

[18] M. Teresa Pontes, Ricardo Aguiar, and H. Oliveira Pires. A nearshore wave energy atlas for Portugal. *Journal of Offshore Mechanics and Arctic Engineering*, 127(3):249–255, 2005.

[19] Rafael Waters, Jens Engstrom, Jan Isberg, and Mats Leijon. Wave climate off the Swedish west coast. *Renewable Energy*, 34(6):1600–1606, 2009.

[20] Eugen Rusu and C. Guedes Soares. Numerical modelling to estimate the spatial distribution of the wave energy in the Portuguese nearshore. *Renewable Energy*, 34(6):1501–1516, June 2009.

[21] L. Rusu, P. Pilar, and C. Guedes Soares. Hindcast of the wave conditions along the west Iberian coast. *Coastal Engineering*, 55(11):906–919, 2008.

[22] Andrew Cornett. Inventory of Canada's marine renewable energy resources. Technical Report CHC-TR-041, National Research Council - Canadian Hydraulics Centre, Ottawa, K1A 0R6, Canada, April 2006.

[23] B. Golding. A wave prediction system for real-time sea state forecasting. *Quarterly Journal of the Royal Meteorological Society*, 109(460):393–416, April 1983.

[24] S. Hasselmann, K. Hasselmann, E. Bauer, P.A.E.M. Janssen, and G.J. Komen. The WAM model-a third generation ocean wave prediction model. *Journal of Physical Oceanography*, 18(12):1775–810, December 1988.

[25] H L Tolman. A third-generation model for wind waves on slowly varying, unsteady, and inhomogeneous depths and currents. *Journal of Physical Oceanography*, 21(6):782–97, 1991.

[26] S. Ponce de Len and C. Guedes Soares. On the sheltering effect of islands in ocean wave models. *J. Geophys. Res.*, 110(C9):C09020–, September 2005.

[27] S. Ponce de Len and C. Guedes Soares. The sheltering effect of the Balearic Islands in the hindcast wave field. *Ocean Engineering*, 37(7):603–610, May 2010.

[28] Philip L.-F. Liu and Inigo J. Losada. Wave propagation modeling in coastal engineering. *Journal of Hydraulic Research*, 40(3):229–240, 2002.

[29] M.T. Pontes. Onshore wave energy resource. methodology and tools for the assessment. In *Proceedings of the International Offshore and Polar Engineering Conference*, volume 1, pages 575–575, Hague, Netherlands, 1995. Int Soc of Offshore and Polar Engineerns (ISOPE).

[30] H.N. Southgate. The use of wave transformation models to evaluate inshore wave energy resource. In *European Wave Energy Synposium*, 1993.

[31] N. Booij, R.C. Ris, and L.H. Holthuijsen. A third-generation wave model for coastal regions. 1. model description and validation. *Journal of Geophysical Research*, 104(C4):7649–66, April 1999.

[32] James T. Kirby and Robert A. Dalrymple. A parabolic equation for the combined refractio-diffraction of Stokes waves by mildly varying topography. *Journal of Fluid Mechanics Digital Archive*, 136(-1):453–466, 1983.

[33] R.C. Ris, L.H. Holthuijsen, and N. Booij. A third-generation wave model for coastal regions. 2. verification. *Journal of Geophysical Research*, 104(C4):7667–81, April 1999.

[34] Richard Allard, W. Erick Rogers, Suzanne N. Carroll, , and Kate V. Rushing. Validation Test Report for the Simulating Waves Nearshore Model (SWAN) Cy-

cle III, Version 40.11. Formal Report NRL/FR/7320–04-10,070, Naval Research Laboratory, 2004.

[35] Y.L. Hsu, J.K. Kaihatu, and A. MacNaughton. Validation test report for coastal wave refraction and diffraction model. NRL formal report NRL/FR/7322-97-9664, Naval Research Laboratory, 1997.

[36] James M. Kaihatu. Review and verification of numerical wave models for near coastal areas - part 2: Verification of numerical wave models. Technical report, Naval Research Laboratory, November 7 1997.

[37] Sang-Ho Oh, Kyung-Duck Suh, Sang Son, and Dong Lee. Performance comparison of spectral wave models based on different governing equations including wave breaking. *KSCE Journal of Civil Engineering*, 13(2):75–84, March 2009.

[38] Colin Andrew. Bibliographic review of nearshore wave models. Technical report, Maritime Operations Division Aeronautical and Maritime Research Laboratory, July 1999.

[39] Christopher J. Bender and Robert G. Dean. Wave field modification by bathymetric anomalies and resulting shoreline changes: a review with recent results. *Coastal Engineering*, 49(1-2):125–153, August 2003.

[40] Jerome P. Y. Maa, T. W. Hsu, C. H. Tsai, and W. J. Juang. Comparison of wave refraction and diffraction models. *Journal of Coastal Research*, 16(4):1073–1082, 2000.

[41] Jose M. Grassa and Jorge Flores. Discussion of: Maa, J.P.-Y.; Hsu, T.-W.; Tsai, C.H., and Juang, W.J., 2000. Comparison of Wave Refraction and Diffraction Models. *Journal of Coastal Research*, 17(3):762–764, 2001.

[42] A.C. Radder. On the parabolic equation method for water-wave propagation. *Journal of Fluid Mechanics*, 95:159–76, November 1979.

[43] James M. Kaihatu. Review and verification of numerical wave models for near coastal areas - part 1: Review of mild slope equation, relevant approximations, and technical details of numerical wave models. Technical report, Naval Research Laboratory, November 7 1997.

[44] D.K.P. Yue and C.C. Mei. Forward diffraction of Stokes waves by a thin wedge. *Journal of Fluid Mechanics*, 99:33–52, July 1980.

[45] James M. Kaihatu, W. Erick Rogers, Y. Larry Hsu, and William C. O'Reilly. Use of phase resolving numerical wave models in coastal areas. Technical report, National Research Laboratory, January 1998.

[46] James T. Kirby, Robert A. Dalrymple, and Fengyan Shi. *REF/DIF 1 v3.0 Documentation and User's Manual*. Center for Applied Coastal Research, Department of Civil and Environmental Engineering, University of Delaware, Newark, DE 19716, 3.0 edition, September 2002.

[47] The SWAN team. *SWAN User Manual*. Delft University of Technology, P.O. Box 5048 2600 GA Delft The Netherlands, 2006.

[48] R. F. Henry and R. A. Walters. Geometrically based, automatic generator for irregular triangular networks. *Communications in Numerical Methods in Engineering*, 9(7):555–566, 1993. I have printed and read this paper.

[49] Coastal Engineering Research Center (U.S.). *Shore protection manual / U.S. Army Coastal Engineering Research Center*. The Center ; for sale by the Supt. of Docs., U.S. Govt. Print. Off., Fort Belvoir, Va. : Washington :, 3d ed. edition, 1977.

[50] The Department of Fisheries and Oceans. Webtide tidal prediction model. `http://www2.mar.dfo-mpo.gc.ca/science/ocean/coastal_hydrodynamics/WebTide/webtide.html`, 2010. Viewed August 23.

[51] Paul C. Liu. A representation for the frequency spectrum of wind-generated waves. *Ocean Engineering*, 10(6):429–441, 1983.

[52] A.V. Boukhanovsky and C. Guedes Soares. Modelling of multipeaked directional wave spectra. *Applied Ocean Research*, 31(2):132–141, April 2009.

[53] Jeffrey L. Hanson, Hendrik Tolman, Barbara A. Tracy, and R. Douglas Scott. Pacific hindcast performance evaluation of three numerical wave models. In *Proceedings of the 9th International Workshop on Wave Hindcasting and Forecasting*, September 2006.

[54] Joao Cruz. *Ocean Wave Energy*. Number 1865-3529 in Green Energy and Technology(Virtual Series). Springer Berlin Heidelberg, 2008.